FREQUENCY SELECTIVE SURFACES FOR TERAHERTZ APPLICATIONS

A THESIS SUBMITTED TO
THE GRADUATE SCHOOL OF ENGINEERING AND SCIENCE
OF BILKENT UNIVERSITY
IN PARTIAL FULFILLMENT OF THE REQUIREMENTS FOR
THE DEGREE OF
MASTER OF SCIENCE
IN
ELECTRICAL AND ELECTRONICS ENGINEERING

By
Mehrab Ramzan
August, 2015

FREQUENCY SELECTIVE SURFACES FOR TERAHERTZ APPLICATIONS

By Mehrab Ramzan

August, 2015

We certify that we have read this thesis and that in our opinion it is fully adequate, in scope and in quality, as a thesis for the degree of Master of Science.

Assist. Prof. Dr. Ali Kemal Okyay (Advisor)

Dr. Kağan Topallı (Co-Advisor)

Assist. Prof. Dr. Necmi Bıyıklı

Assoc. Prof. Dr. Mustafa Seçmen

Approved for the Graduate School of Engineering and Science:

Prof. Dr. Levent Onural
Director of the Graduate School

ABSTRACT

FREQUENCY SELECTIVE SURFACES FOR TERAHERTZ APPLICATIONS

Mehrab Ramzan
M.S. in Electrical and Electronics Engineering
Advisor: Assist. Prof. Dr. Ali Kemal Okyay Co-Advisor: Dr. Kağan Topallı
August, 2015

This thesis presents Terahertz (THz) Frequency selective surfaces (FSS) that can be realized using standard microfabrication techniques. These FSS structures are designed for frequencies around 0.8 THz, which is a crucial operating frequency in security and medical imaging. Using THz waves for such applications, multilayer frequency selective surfaces are preferred due to their wide flat band response, lower dependency to angle of incidence, and low loss. The implementation of such structures requires very thin layers of substrates and membranes in order to improve the performance in THz regime. In order to alleviate the difficulty in the implementation of multilayer structures, a fabrication process is proposed where a 100 μm-thick glass membrane is formed through HF etching of a 500 μm-thick glass wafer. Using this fabrication process, three separate designs consisting of single-layer FSS are investigated using high frequency structural simulator (HFSS). The first design, consists of a circular ring slot in a square metallic structure on top of a 100 μm-thick Pyrex glass membrane with 95% transmission bandwidth of approximately 0.042 THz , which remains nearly constant till 30^o angle of incidence. The second design consists of a tripole structure on top of a 100 μm-thick Pyrex glass membrane with nearly 95% transmission bandwidth of 0.015 THz, which remains nearly constant till 30^o angle of incidence. The third structure consists of a triangular ring slot in a square metal on top of a 100 μm-thick Pyrex glass membrane with 95% transmission bandwidth of 0.015 THz, which remains nearly constant upto 20^o angle of incidence. These designs show that the reflections from samples can be reduced compared to the conventional sample holders used in THz spectroscopy applications; by using single layer FSS structures manufactured through a relatively simple fabrication process.

Keywords: FSS, band-pass filters, band-stop filters , low pass filters, high pass filters, spatial filters, absorbers, metamaterials, fabrication, glass, Terahertz.

ÖZET

TERAHERTZ UYGULAMALARI İÇİN FREKANS SEÇİCİ YÜZEYLER

Mehrab Ramzan
Elektrik ve Elektronik Mühendisliği, Yüksek Lisans
Tez Danışmanı: Yrd. Doç. Dr. Ali Kemal Okyay
Tez Eş-Danışmanı: Dr. Kağan Topallı
Ağustos, 2015

Bu tez, standart mikrofabrikasyon teknikleri kullanılarak üretilebilecek Terahertz (THz) frekans seçici yüzeyleri (FSY) içermektedir. FSY yapıları medikal görüntüleme ve güvenlik uygulamaları için kritik önem arz eden 0.8 THz yakınındaki frekans değerlerine uygun olacak şekilde tasarlanmıştır. Bu tür uygulamalarda THz dalgaları kullanıldığında, çok katmanlı FSY yapıları geniş düz bant yanıt değerleri, geliş açısından düşük düzeyde etkilenmeleri ve düşük kayıp düzeyleri sebebiyle tercih edilmektedir. THz bölgesinde performansı geliştirmek amacıyla üretilen bu yapılar çok ince alt katman ve membranların kullanımını gerektirmektedir. Çok katmanlı yapıların üretimindeki bu zorluğu azaltmak amacıyla, 100 μm kalınlığındaki cam membran yapının 500 μm kalınlıktaki bir cam parçadan HF tabanlı asidik aşındırmayla elde edilmesini içeren bir fabrikasyon işlemi önerilmiştir. Bu fabrikasyon işlemi kullanılarak tasarlanan üç farklı tek katmanlı FSY, yüksek frekans yapısal simülatör (HFSS) ortamında araştırılmıştır. İlk tasarım %95 geçirgenliğe sahip olan 0.042 THz bant aralığına sahip, bu bant aralığı 30 derecelik geliş açısına kadar sabit kalmaktadır. Bu tasarımda 100 μm kalınlıktaki Pyrex cam membran üzerinde yer alan kare şeklindeki metal yapı içerisindeki çembersel bir halka yarığından oluşur. İkinci tasarım %95 geçirgenliğe sahip olan 0.015 THz bant aralığına sahip, bu bant aralığı 30 derecelik geliş açısına kadar sabit kalmaktadır. İkinci tasarım, 100 μm kalınlıktaki Pyrex cam membran üzerinde yer alan üç kutuplu bir yapıyı içermekte iken, üçüncü tasarım %95 geçirgenliğe sahip olan 0.015 THz bant aralığına sahip, bu bant aralığı 20 derecelik geliş açısına kadar sabit kalmaktadır. Üçüncü tasarım, 100 μm kalınlıktaki Pyrex cam membran üzerinde yer alan üçgensel halka yarığın yer aldığı kare şeklindeki bir metalden oluşmaktadır. Bu tasarımlar, THz spektroskopi uygulamalarında hali hazırda kullanılan örnek taşıyıcılardaki

yansımaların daha basit fabrikasyon metotları ile üretilen tek katmanlı FSY yapıları kullanılarak daha az düzeylere indirilebileceğini göstermektedir.

Anahtar sözcükler: Frekans seçici yüzey, bant geçirgen filtreler, bant durdurucu filtreler, düşük frekans geçirgen filtreler, yüksek frekans geçirgen filtreler, uzamsal filtreler, metamalzemeler, fabrikasyon, cam, Terahertz.

Acknowledgement

I would like to express my heartfelt appreciation and gratitude to my supervisor Dr. Ali Kemal Okyay for the patient guidance, encouragement and advice he has provided throughout my time as his student. I have been so lucky to have a supervisor who cared so much about my work, and who responded to my questions and queries all of the time. Throughout MS research, he was so polite, friendly, and never become angry at me.

I would like to thank Dr. Kağan Topallı for being my co-supervisor and for his precious time, help, reviews, and comments throughout the year.

I would like to thank Dr. Necmi Bıyıklı for not only being member of the jury, reading and reviewing my thesis but also for the fabrication course offered at material science, which made me capable of writing the fabrication process of my design.

I would also thank Dr. Mustafa Seçmen from Yasar University for reading, reviewing and being the member of my jury. I am also thankful to him for his precious time and traveling long way from Izmir to Ankara for my thesis defense.

I would like to thank to the Okyay group members: Sami Bolat, Fatih Bilge Atar, Amir Gobadi, Enes Battal, Muhammad Maiz Ghauri, Turkan Gamze Ulusoy, Burak Tekcan, Seyma Canik, Amin Nazirzadeh, Abdullah Gok, Sina Abedini Dereshgi, Hasan Karaca and Ozan Onur elik. They are all like family members to me and I thank them all with the core of heart for their encouragement and help.

I would like to thank dorm 15 brothers: Abdul Ali, Tufail Ahmed, Saghir Abbas, Shahid Ali, Asad Ali, Zulfikar, Ateeq Ur Rehman, and Mubim Memom. They

are all very encouraging and caring persons to me.

I would like to thank to the organization of Higher education commission (HEC), Pakistan for supporting my expenses during my MS program.

Finally, I would like to thank my family and friends for their support, co-operation, and patience.

Contents

List of Figures

List of Tables

Chapter 1

Introduction

1.1 FSS definition

From electromagnetic point of view, FSS are essentially resonant periodic arrays which exhibit selectivity in frequency, polarization, and angle of incidence. In contrast to electrical filters, FSS are spatial filters because their performance depends not only on frequency, but also on angle and polarization of the incident wave [1]. A periodic array consisting of conducting patch or aperture [2] [3] elements is known as frequency selective surface or dichroic [4]. Generally, they are employed as plane-wave filters at radio, microwave, and THz frequencies.

1.2 Applications

These kind of structures can be used in the manufacturing of hybrid radomes, dichroic subreflectors, circuit analog absorbers, and meanderline polarizers [5]. A very common example of FSS is periodic array of metallic holes used for designing microwave oven screens used for reflecting energies at 2.45 GHz and allowing light to pass through so that food can be seen while being cooked [4]. Hybrid

radomes are like band-pass radomes used for decreasing radar cross section (RCS) of antenna outside the operating frequency. Dichroic subreflector for two different operating frequencies allow us to use one main reflector rather than two, which helps us in decreasing the size, weight, and complexity of the overall system.

A lot of work has been done and explored in microwave and higher frequency regimes such as infrared/optical spectrum [6]. However, for long past years the frequency gap between microwave and infrared regime remained unexplored due to lack of good sources and detectors and it was commonly referred to as "THz gap" [7]. In recent years, THz region has gained great attention due its useful applications in the space sciences, communication, and sensing [6] [8]. The interest in THz spectrum is increasing because its wavelength is much smaller than microwave region, that provides a very high resolution [8] [9]. Apart from that, the penetration of wave into opaque objects and unique signatures of materials made this region more fascinating for security applications [10]. The non ionization of THz spectrum made it ideal for medical imaging techniques [11]. THz radiations are preferred over X-rays for a number of reasons. Firstly, radiations in this regions are not detrimental to human health due to their less ionization nature. Secondly, they provide better contrast for soft tissues than X-rays in medical applications because THz radiation is very sensitive to polar substances such as water and hydration substances [7].

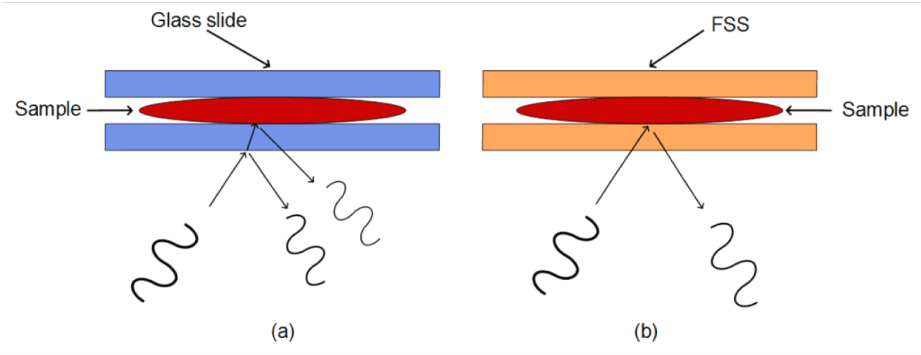

Figure 1.1: Typical measurement setup of the reflections from a biological tissue sample using (a) Glass slide as a sample holder and (b) FSS as a sample holder [12].

There are numerous THz imaging devices commercially available, but the deficiency of handful and smartly developed imaging tools is still a major concern. Furthermore, the low power sources available in THz spectrum present us with unique challenges in THz spectroscopy [12]. In THz measurement setup of reflections from samples such as biological tissues and liquid and powdered specimen are kept in a sample holder. The available glass slide sample holders have severe power losses. Figure 1.1 shows the reflection measurement setup from a biological tissue sample, in case of using glass slider as a specimen holder we loose much of the incident power before striking the sample due to inevitable reflections at the air-glass interface (Figure1.1(a)). FSS structures with transparent qualities, play a very vital role to suppress the unavoidable reflections without compromising the power of incident striking wave (Figure 1.1(b)).The design of these patterns require special care, which should have minimum reflections, maximum transmission, and at the same time its response should be independent of certain angles of incidence [13]. The motivation of this thesis is to provide implementation of such FSS designs which have more than 95% max transmission at central frequency and their results are independent of certain angles of incidence. Additionally, an acceptable design membrane fabrication process is propose which makes this idea more practicable. This design can also replace conventional z-cut quartz crystal in the imaging system for THz applications.

1.3 Thesis outline

The structure of the thesis is as following:

In Chapter 1, definition of frequency selective surface is covered followed by discussion of some general applications of FSS. Furthermore, its applications in THz regime are discussed where we also need some absorbers, band-pass filters and band-stop filters for different purposes.

In Chapter 2, a detailed explanation of some basic FSS structures is given. Initially, depending on the polarization of incident wave the behavior of metallic

horizontal and vertical bars and their equivalent circuits are mentioned. Equivalent circuit models of metallic mesh grids and metal squares are also illustrated.

In Chapter 3, initially two absorbers (metamaterial and cross dipole) in Thz regime are covered. Their design methodology is discussed followed by their reflection and transmission coefficient at normal and different angles of incidence. After that multiple layer bandpass filters results at different angles of incidence in THz regime are discussed. The first bandpass filter consists of a cross layer on polyethylene substrate being sandwiched between two square layers on polyethylene wafers. The second structure, consists of three layers with complement of printed fan type structure sandwiched between printed structures. Finally, their fabrication design constraints are discussed.

In Chapter 4, how to implement a single layer bandpass filter is discussed which makes the design relatively simple and gives us more flexibility in THz in terms of fabrication. The flow of design in the fabrication process is explained in the end. In THz regime, we need very thin substrates comparable to the wavelength of the wave. In order to have nearly perfect matching with the air impedance, to avoid excitation of surface waves, and to downturn the ripples in passband of the design. However, these thin films are very fragile to fabricate different structures on top of them. In order to provide robustness to the design, wet etching of the Pyrex glass with HF as the etchant is explained. This fabrication process lead to anchor points at the corner of the substrate to provide mechanical support to the thin film and making the fabrication process much simpler.

In Chapter 5, the conclusion of the thesis with some future work is discussed.

Chapter 2

Frequency selective surfaces

Frequency selective surfaces (FSS) are periodic structures that reflect, transmit or absorb electromagnetic waves. In other words, they are spatial filters that block, allow or absorb frequencies [4]. Depending on the structure type and geometry the surface can act as bandpass, bandstop, low-pass or high-pass filters [14] [15]. FSS have numerous applications. For instance, they are used in manufacturing hybrid radomes, dichroic subsreflectors, circuit analog absorbers, etc [5]. According to [5], based on the shapes and geometry the structures are divided into four groups of elements as shown in Figure 2.1. Group 1 elements are known as N pole or center connected, the most famous structures are straight element, three-legged element, anchor elements, etc. Group 2 elements are known as loop type elements, the most famous structures in this category are circular, hexagonal and square loops. Group 3 elements are known as solid interior or plate type structures. Last group (Group 4) consists of structures that are combination of structures of all the previous groups. Some elements inherently have wide bandwidth. The structures are arranged in groups from left to right are in the order increasing bandwidth.

In order to understand the concept of FSS let us imagine an electron in a plane, that is only allowed to move in vertical direction as shown in Figure 2.2 and a plane wave is normal incident upon it, whose E-field lies in the source of the

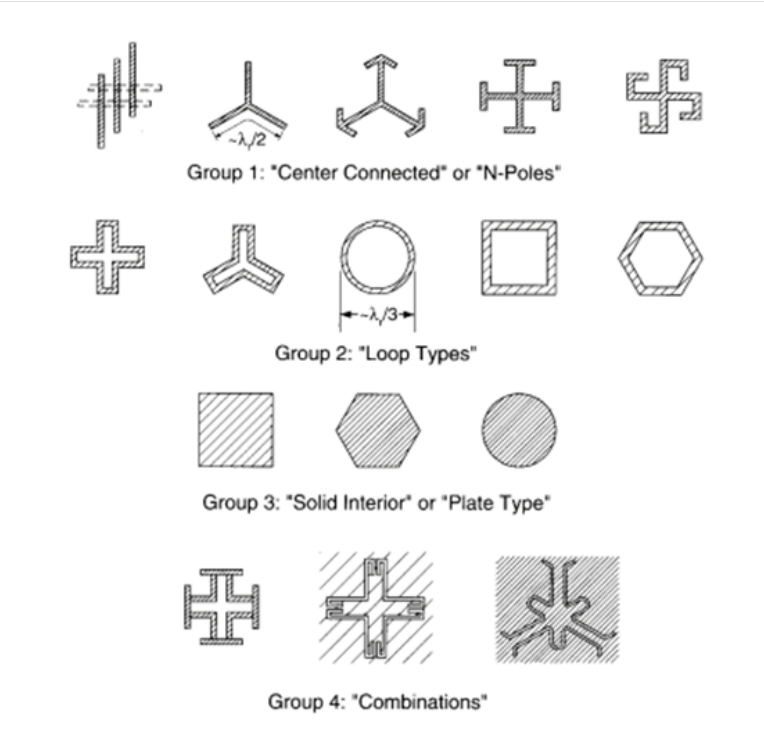

Figure 2.1: Different structures used for frequency selective surfaces [5].

plane. The E-field will exerts a force on the electron and causes it to oscillate. As a result some part of the source energy is transfered to electron as kinetic energy which allows it to oscillate. According to law of conservation of energy, some part incident will be transmitted and remaining power will be absorbed by the electron. If all the energy is transferred to the electron then the transmittance through the structure will be zero.

Now let us imagine a slightly different scenario as shown in Figure 2.3. The E-field of incident plane wave is still in the same direction, however electron is restricted to move along a horizontal wire. In this case, the electron is fully invisible to the incident wave and the striking wave will transmit through filter because the exerted force can't oscillate the electron in the horizontal direction. To summarize, we can say that if the energy is absorbed by the electron the transmittance is low whereas if the energy is not absorbed then the transmittance through the structure is very high. But what happens to the incident wave which is not transmitted. In case of low transmittance, the oscillating electron will act

as an electric dipole and as a result will radiate perpendicular to the oscillation axis. As the radiation will be on both sides (left and right) of the filter, the emitted radiation on the right side will destructively interfere with wave coming from the left, resulting in zero transmittance. The radiation on the left side of diagram is referred to as reflected wave. In general, the transmittance through the structure is highly depended on frequency, in other words, the electrons in metals will absorb and re-radiate some wavelengths with higher efficiency than others. The shape of the transmittance curve is highly depended on the dimensions and patterns etched on the metal part of the structure.

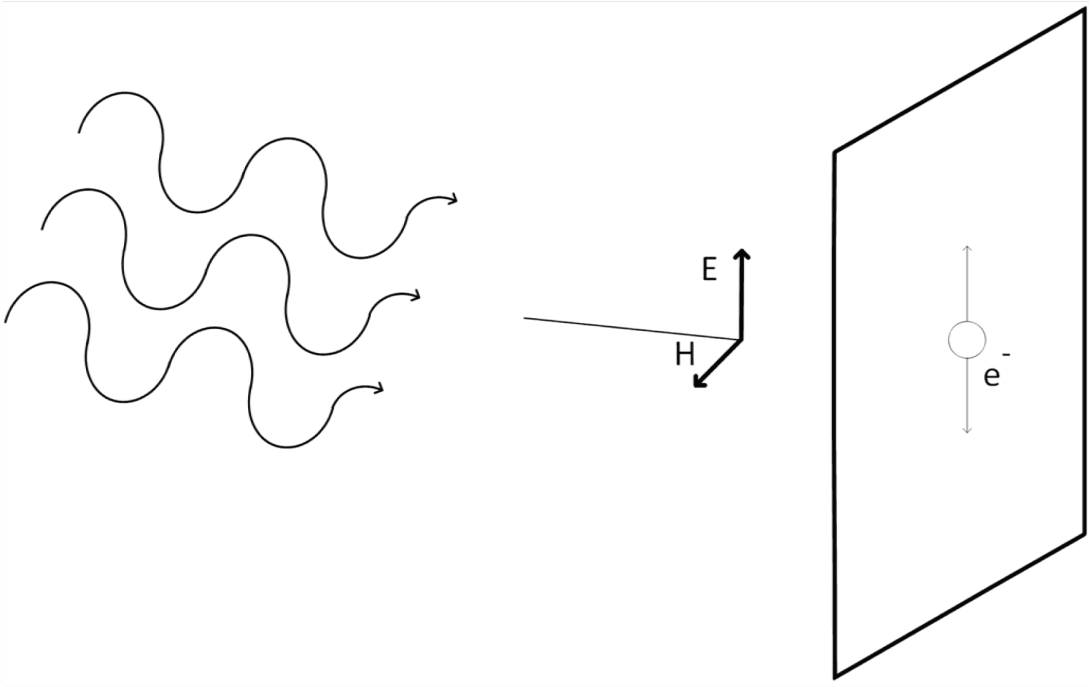

Figure 2.2: A vertically polarized plane wave striking the filter plane and causing oscillation to an electron in E-field direction.

2.1 FSS structures and equivalent circuits

The most common used structures in FSS are strip grating filters, mesh filters, and cross mesh filters. Initially the discussion will be about strip grating filter which is used as the fundamental structures to explain most complicated structures.

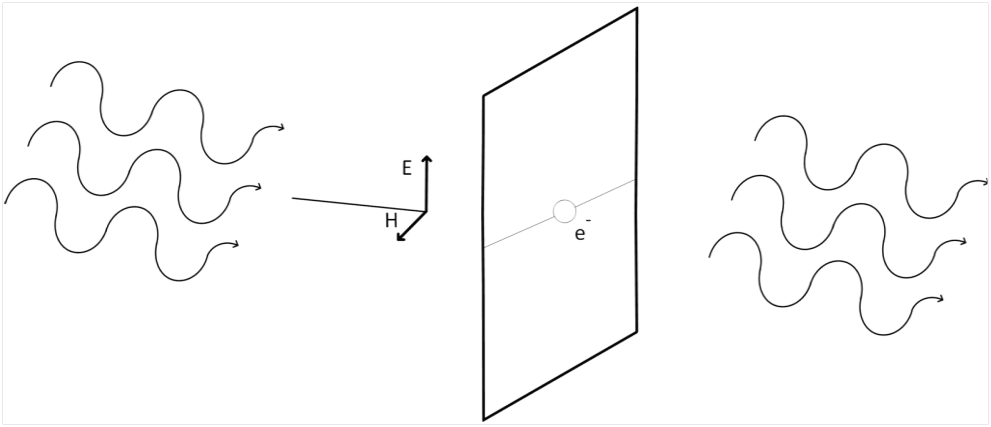

Figure 2.3: A vertically polarized plane wave striking the filter plane and causing no oscillation to an electron in E-field direction.

Furthermore, the mesh filters are discussed which are polarization independent structures. Finally, the cross mesh structures are discussed which can be used as band-pass and band-stop filters.

2.1.1 Strip grating structures

The structures of strip grating filter [16] are shown in Figure 2.4 and Figure 2.5.If the E-field is parallel to the metallic strips then it will act as an inductive strip grating filter [17]; if the E-field is perpendicular to metallic strips it will behave as capacitive strip grating [18]. The incident E-field which is perpendicular to metallic strips in capacitive strip grating case undergoes a sinusoidal variation which induces the electrons in metal to oscillate in the same direction. The electrons in metals will move back and forth and will switch states as shown in Figure 2.6. If we consider two cases of monochromatic waves striking this structure, one source is having low frequency (long wavelength as compare to spacing between the grid) and other source with high frequency (shorter wavelength with respect to spacing between the grids). In first case, initially the strip filter is neutral if the longer wavelength source strikes it will drive it into one of the two charge states. The structure will remain in that state until the direction of E-field is reversed and change the current direction in the opposite way [18]. As the low frequency source varies very slowly so the electrons remain stationary for long

time and do not absorb much energy from the source during these periods. As a result, small portion of energy will be absorbed by the electron and transmittance will be maximum in this case [18].

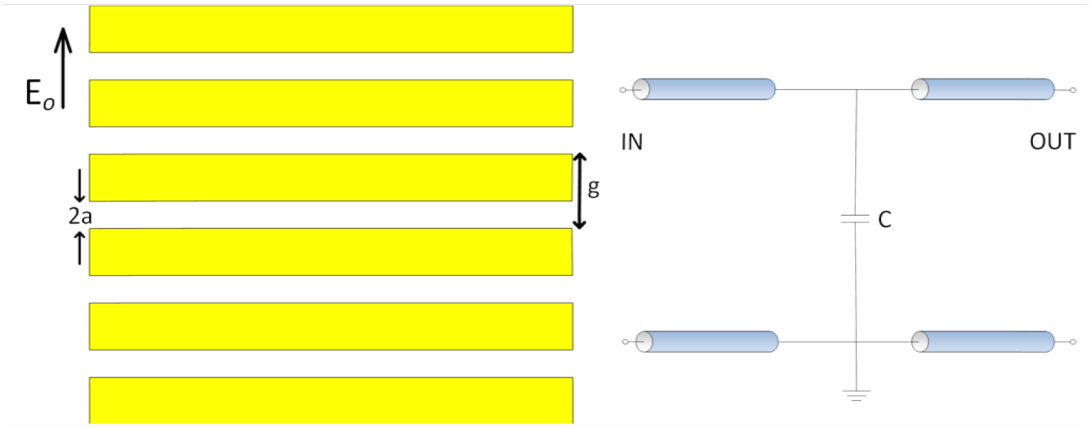

Figure 2.4: Horizontal metallic strips and its equivalent circuit model.

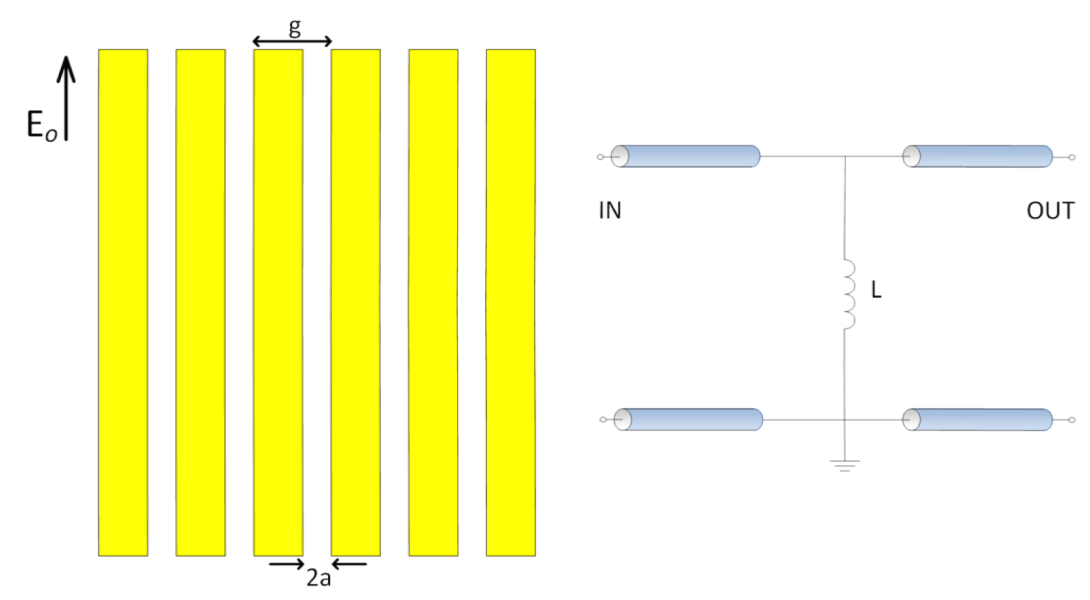

Figure 2.5: Vertical metallic strips and its equivalent circuit model.

In the second case, if a source with high frequency strikes the neutral structures, it will again drive the filter in one of the states. This time the filter will not remain in one of the states for long time but will switch rapidly between the two states because of rapid oscillation of incident E-field. Since the electrons in this structure are oscillating frequently so maximum energy of the incident

wave is being absorbed by the electrons and this will lead to minimum transmittance through the structure. The behavior of this structure resembles like a low pass filter since it transmits at low frequencies and blocks higher frequencies. As a result this structure is modeled as capacitor connected in shunt between the transmission line [19]. A high frequency signal will not reach to output as it will drive current across the capacitor and travel to ground. A low frequency signal will reach to output as it is unable to drive current across the capacitor. For

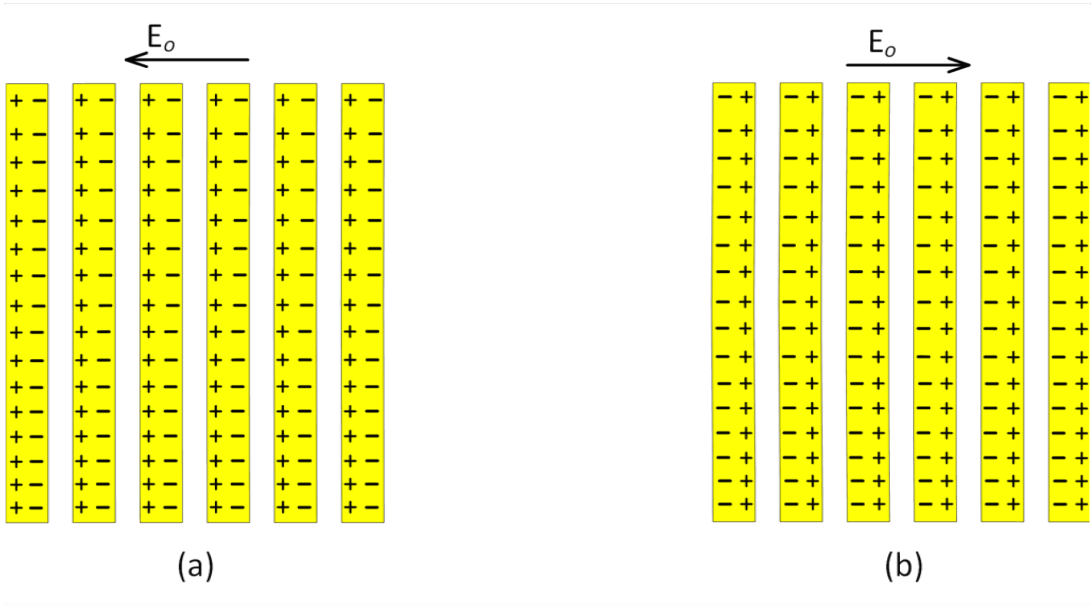

Figure 2.6: Charge distribution on metallic strips with E-field perpendicular to the metallic strips during the (a) negative cycle of striking wave and (b)positive cycle of striking wave.

second example where the E-field is parallel to strips as shown in Figure 2.7 we also consider the same two cases to analyze its behavior. In the first case if low frequency signal strikes the structures it will drive structure from neutral state to one of the two states. The electrons along the metallic strips will continue to move until the E-field reverse its directions. This time the electrons will continue to move as they are moving along the longer dimension of the metallic strips. Therefore, the transmittance through the structure will be minimum as the most of the energy is transfered to the electrons. In the second case of short wavelength source, the incident wave will make the electrons to oscillate. This time, the electrons move only a small distance before they change the direction. The electrons

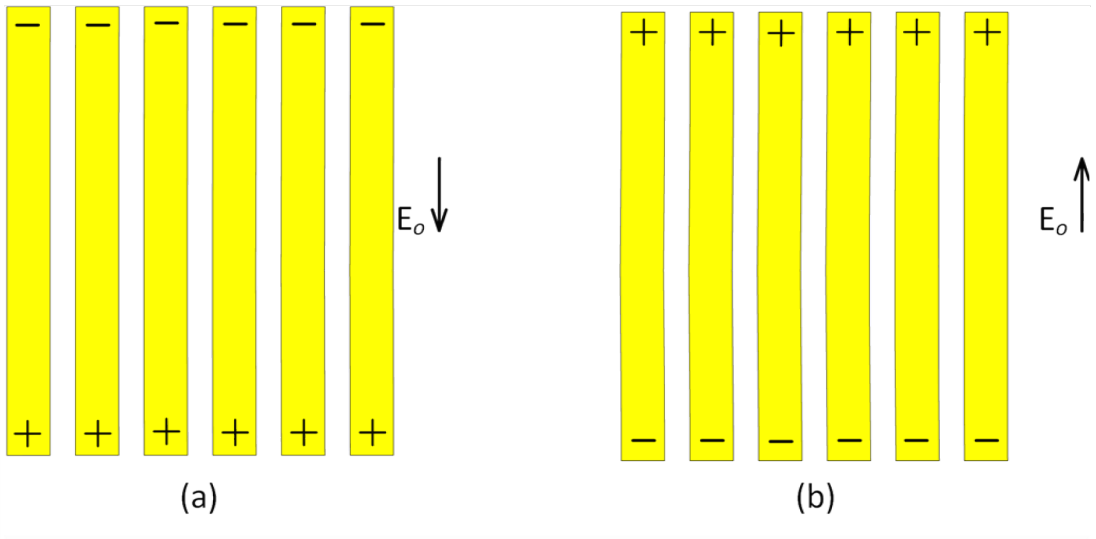

Figure 2.7: Charge distribution on metallic strips with E-field parallel to the metallic strips during the (a) negative cycle of striking wave and (b) positive cycle of striking wave.

wiggle back and forth at high frequency but fail to exhibit the long-range motion excited by the long-wavelength source. Therefore the absorption will be smaller and transmittance will be very high. The behavior of this structure resembles as that of high pass filter. This structure is modeled as an inductor shunt connected to the ground. At low frequencies there will be no output as the current will drive across the inductor through the ground and high frequencies will unable to drive current across the inductor yielding maximum output.

The major disadvantage of these kind of structure is that they are polarization dependent. As discussed before, if the E-field is perpendicular to the structure it will exhibit capacitive behavior, while the E-field is parallel it will behave like an inductor.

2.2 Mesh Structures

The structures of inductive and capacitive mesh filters are shown in Figure 2.8 and Figure 2.9 [20] [21]. The circuit models of both structure are also given in the

same Figure, which correspond to their response when incident plane wave strikes the structures [22]. R in the circuit models is modeling loss of conductors if a low loss conductor is used for the designs then it can be ignored. The advantage of these structures are that they are independent of the polarization of the incident wave, the structure model will remain the same if it is rotated 90^o.

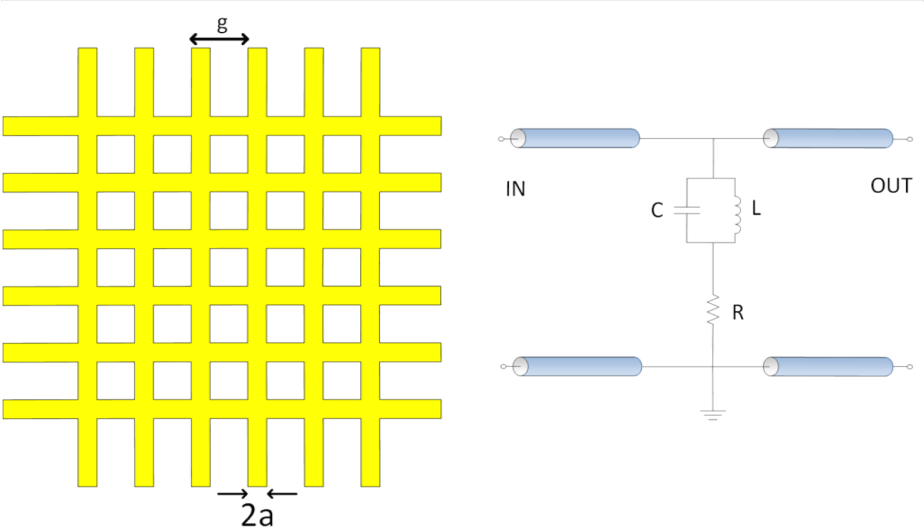

Figure 2.8: Metallic mesh structure and its equivalent circuit model.

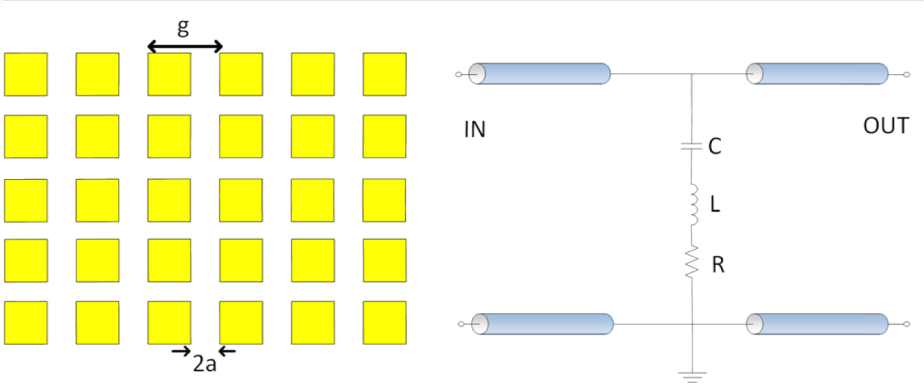

Figure 2.9: Metallic periodic square structure and its equivalent circuit model.

Chapter 3

Simulation of different FSS structures

In this section different frequency selective surfaces will be covered such as absorbers, low pass, high-pass filters, band-pass filter and band stop-filters in THz regime. The parameters of different structures will be discussed and there fabrication constraints will also be highlighted in this section.

3.1 Absorber

Usually finding a strong absorber at THz regime is very difficult. These kind of absorber find wide variety of application such as they can be used as for thermal detectors or as coating material to reduce unwanted reflections when using continuous sources like quantum cascade lasers. The main rule of thumb in designing FSS is to match the impedance of the structure with the air impedance of about 377Ω in order to minimize the reflection coefficient and maximize the transmission coefficient. The impedance matching can be carried by proper controlling the dimensions of the unit structure and choosing an appropriate structure. The structure geometry, inter-element spacing and other dimensions of the FSS play

a very important role in having a desired shape of transmission and reflection coefficient. The idea behind designing an absorber is to minimize simultaneously reflection coefficient and transmission coefficient [23]. In addition to it keeping the absorption close to unity at wide angles of incidence. In this section an absorber is designed which is having absorptivity of 0.97 at 1.6 THz. The advantage of this absorber is that it is flexible as polyimide is used as the substrate with total thickness of about 16 μm which allows it to be easily wrapped around an object with the diameter of about 6 mm. Apart from that this absorber works for wide range of angles for both transverse electric (TE) and transverse magnetic (TM) confiuration of waves.

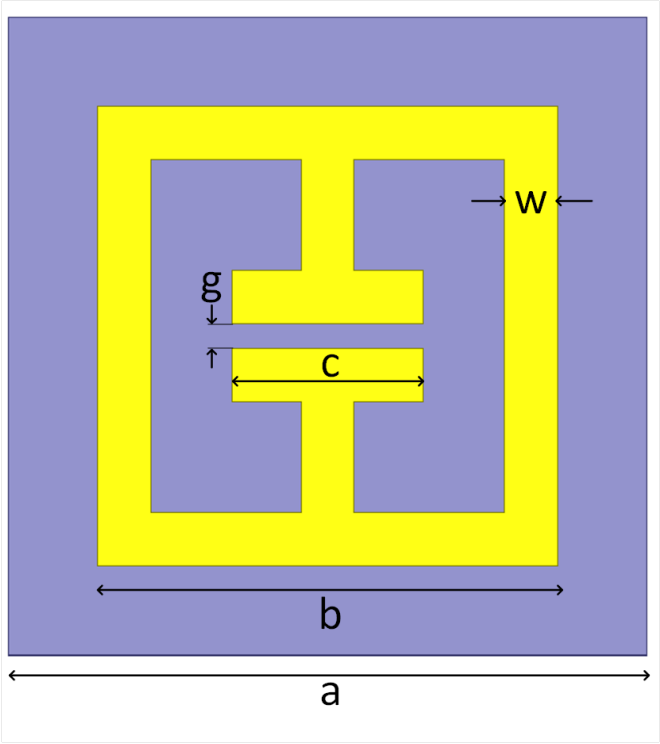

Figure 3.1: Snapshot of unit cell of the metamaterial based absorber and its physical parameters.

The unit cell and array of absorber is shown in Figure 3.1 and Figure 3.2, respectively. Table 3.1 shows the physical parameters of the unit cell of the metamaerial based absorber. The side view of structure is shown in Figure 3.3 which consists of two substrates of polyimide with the relative permittivity of ϵ_r=2.88 and tanδ=0.0313. The bottom dielectric layer below the continuous

metal is for mechanical support so it does not contribute to the results. Each polyimide is having a thickness of 8 μm. The metal used here is lossy gold with the conductivity of $\sigma = 4.09 \times 10^7 S/cm$ and thickness of 200 nm. The absorption coefficient is calculated by using unitary property which is given below as:

$$S_{11}^2 + S_{21}^2 = 1 \tag{3.1}$$

Where S_{11} is the reflection coefficient and S_{21} is the transmission coefficient which is zero throughout the frequency range due the ground plane [23]. The above equation is only satisfied if the structure is lossless. However, the structure here is not lossless so we can use the above unitary property to calculate the absorption coefficient(A) as:

$$A = 1 - S_{11}^2 - S_{21}^2 \tag{3.2}$$

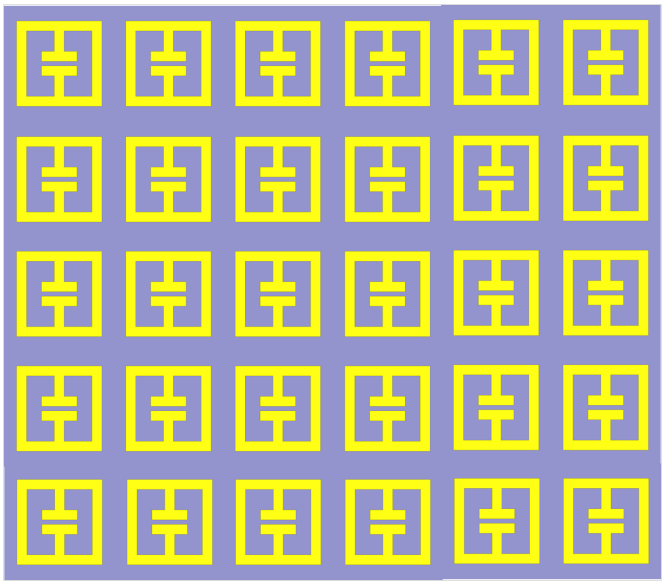

Figure 3.2: Array of the metamaterial based absorber.

Figure 3.4 shows the absorption coefficient results of the absorber. The results seem to be independent of incident angle for TE wave configuration with minimum absorption of approximately 40%. Table 3.2 gives detail information of about incident TE wave configuration absorption coefficient result at different angle of incidence. Figure 3.5 shows the TM wave configuration absorption coefficient

Table 3.1: Physical parameters of the metamaterial based absorber.

Parameters	Values (μm)
a	36
b	25.9
c	10.8
g	1.4
w	3
t_1	8
t_2	8

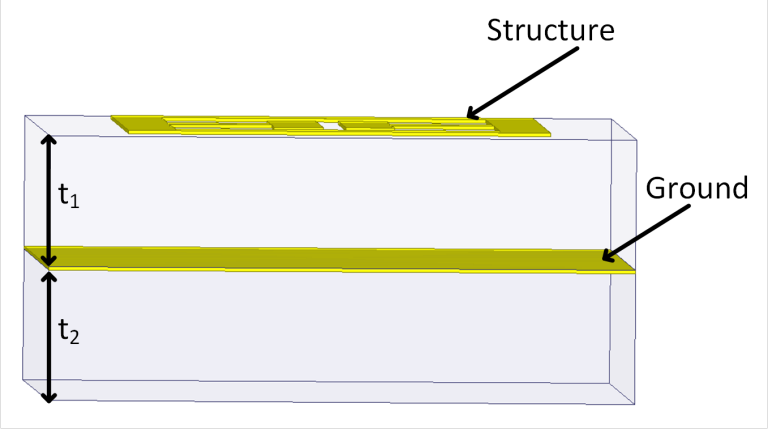

Figure 3.3: Side view of unit cell of the metamaterial based absorber consisting of polyimide substrate.

results. The results are quite good as they are independent of incidence angle and amplitude of absorption is close to unity in all cases. Table 3.3 gives detail information about the absorption coefficient at each angle of incidence.

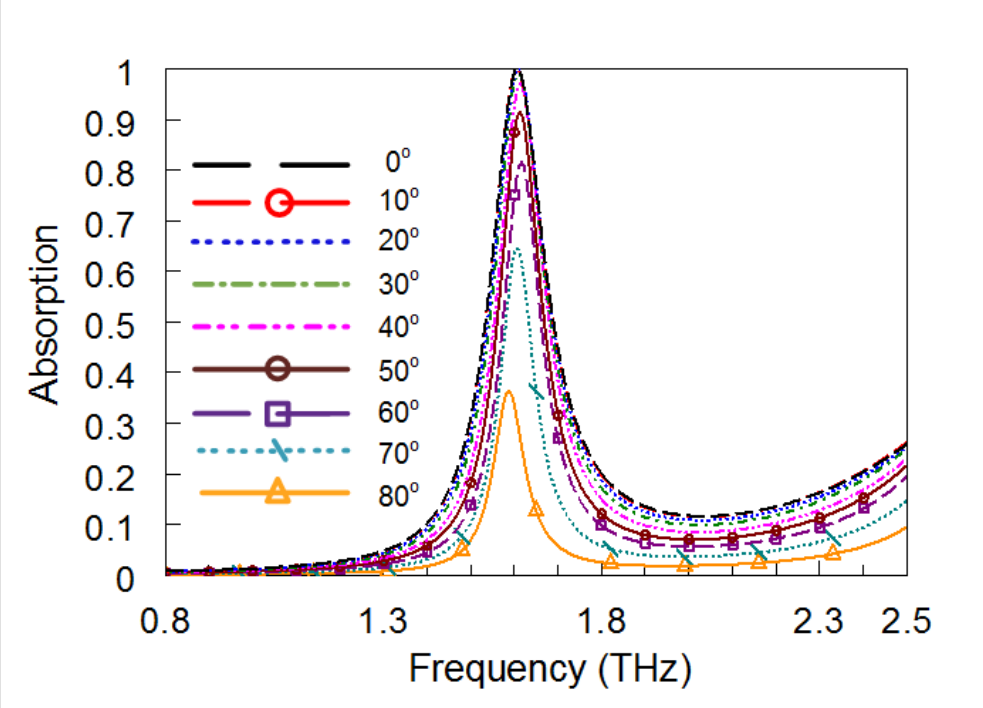

Figure 3.4: HFSS simulation results of the absorption coefficient of the metamaterial based absorber for TE case at different angles of incidence.

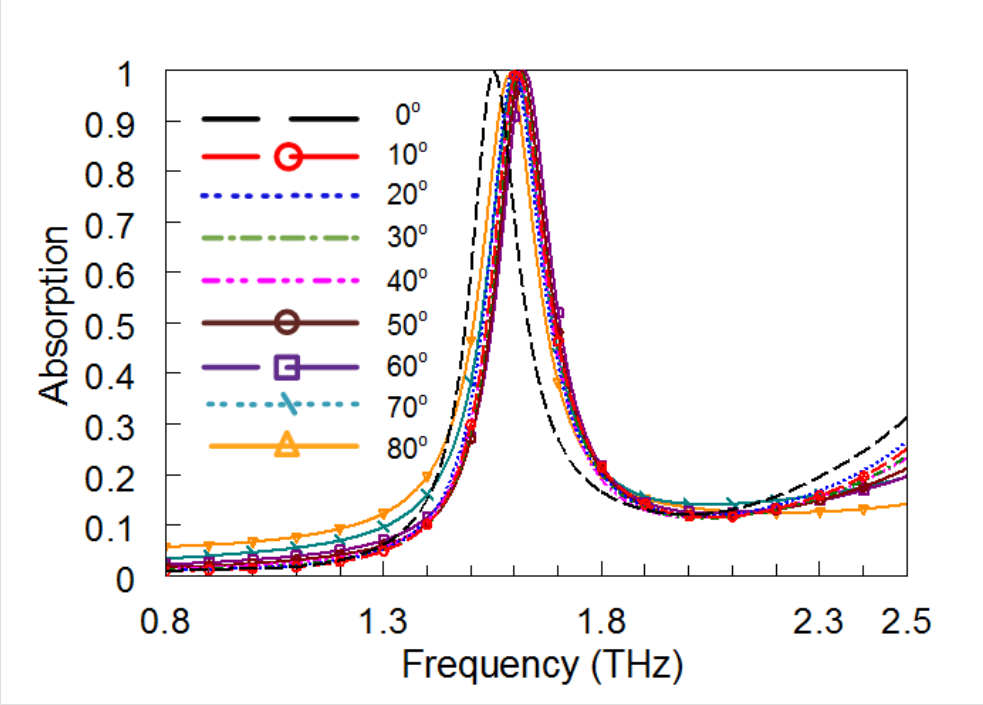

Figure 3.5: HFSS simulation results of the absorption coefficient of the metamaterial based absorber for TM case at different angles of incidence.

Table 3.2: The absorption coefficient values of metamaterial based absorber at different angle of incidence for TE wave configuration.

Angle of incidence (Degrees)	Absorption
0	0.999
10	0.998
20	0.993
30	0.980
40	0.950
50	0.89
60	0.79
70	0.63
80	0.38

Table 3.3: The absorption coefficient values of the metamaterial based absorber at different angle of incidence for TM wave configuration.

Angle of incidence (Degrees)	Absorption
0	0.999
10	0.998
20	0.997
30	0.9994
40	0.99
50	0.98
60	0.991
70	0.997
80	0.997

3.2 Cross dipole absorber at far infrared regime for wide angle of incidence

Metamaterials and periodic structures play important in electromagnetics, as they exhibit certain unique functionality and control the propagation of electromagnetic waves. The have wide variety of applications like negative refractive index materials are used for superlensing [24], cloaking [25], solar cells [26] and miniaturized antennas [27]. In this section, another absorber in far infrared regime will be discussed [28]. The top structure of unit is shown in Figure 3.6 which is simple a cross dipole and its respective array is shown in Figure 3.7. The side view of structure is shown in Figure 3.8 which shows that cross dipole is on top of Silicon Carbide (SiC) layer, below SiC there is a continuous metal layer and at the bottom Si substrate is used. The metal used for the structure is gold with the thickness of 100 nm. The optimized dimensions of the unit cell at which the reflection and transmission are minimized in order to have maximum absorption are given in Table 3.4. The absorption coefficient at normal angle of incidence is given in Figure 3.9 which is nearly having unitary absorption at 30.6 THz. Figure 3.10 shows absorption coefficient results of cross dipole at different angle of incidence from 0^o to 60^o, the maximum reflection coefficient remains at the same frequency, however the magnitude of the absorption coefficient is decreasing slightly below than maximum value.

Table 3.4: Physical parameters of the cross dipole absorber.

Parameters	Values (μm)
L	2.6
W	2.6
L_p	0.4
W_p	1.6
t_m	0.1
t_{SiC}	0.27
t_{Si}	1

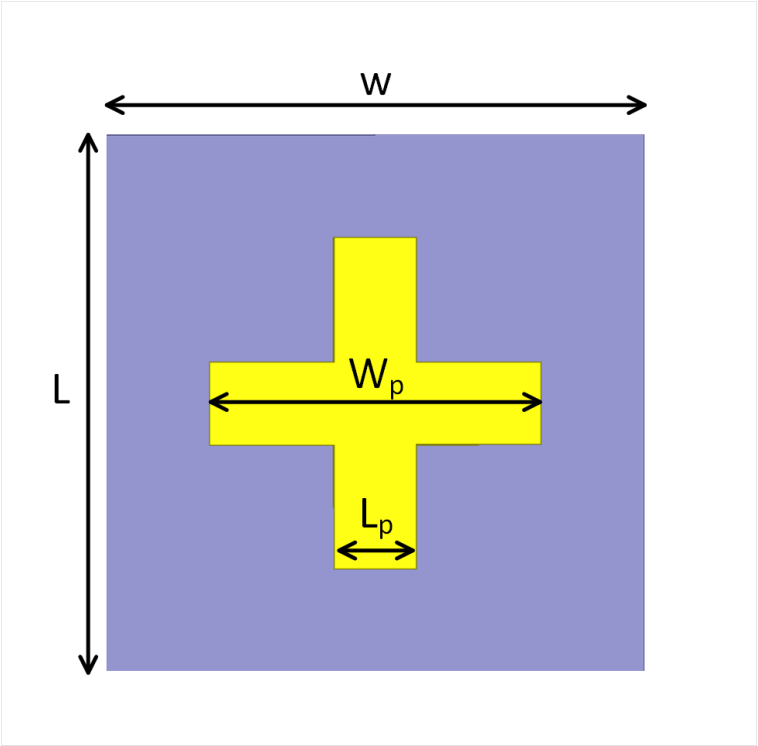

Figure 3.6: The unit cell of the cross dipole absorber.

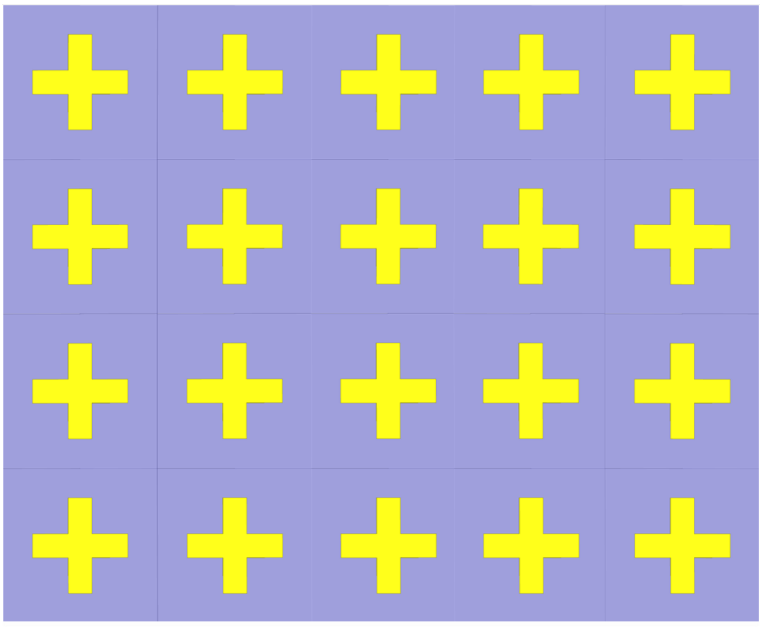

Figure 3.7: The array of the cross dipole absorber.

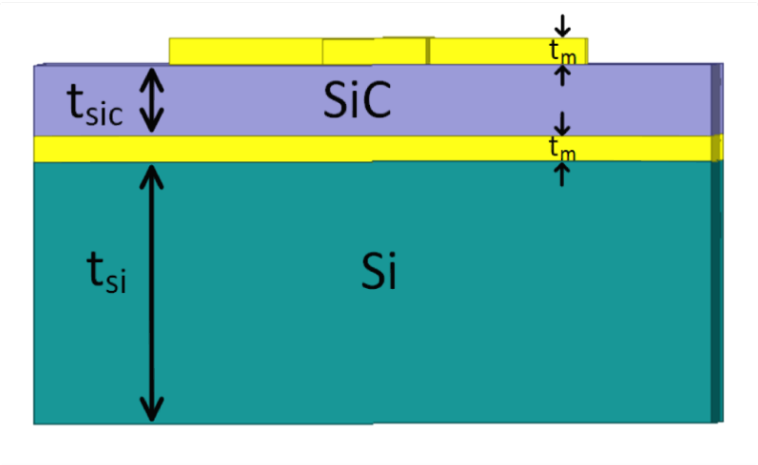

Figure 3.8: Side view of the cross dipole absorber.

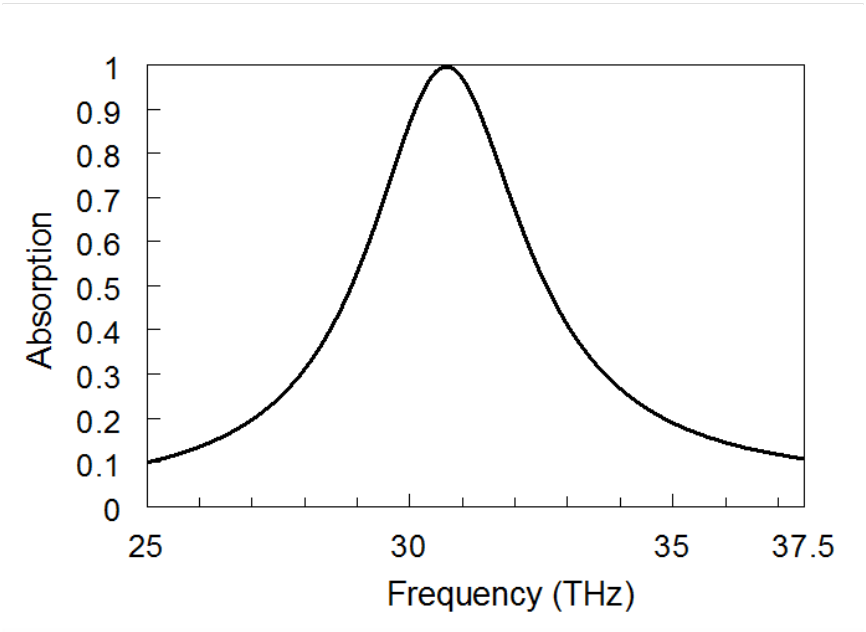

Figure 3.9: HFSS simulation results of the absorption coefficient of the cross dipole absorber at normal angle of incidence.

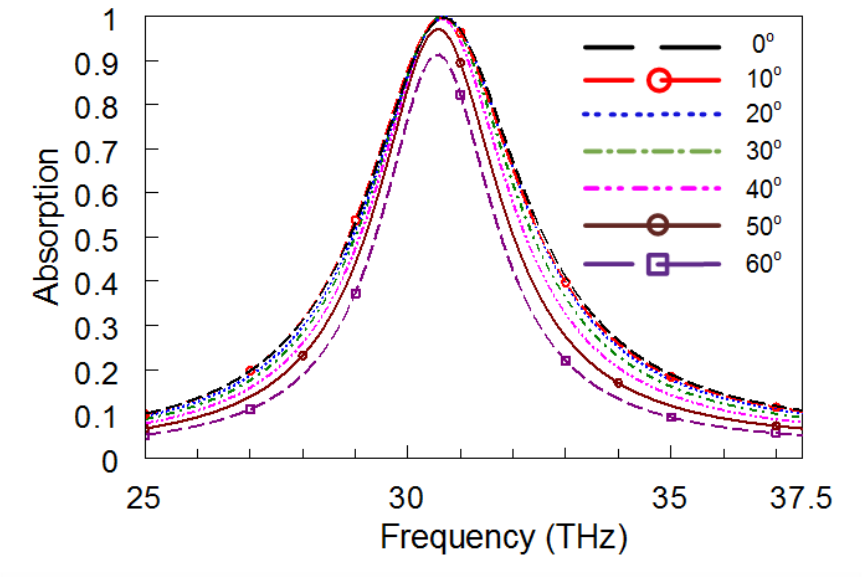

Figure 3.10: HFSS simulation results of the absorption coefficient of the cross dipole absorber at different angle of incidence.

3.3 Multiple layer frequency selective surfaces band-pass filter designs in HFSS environment

THz frequency is preferred because of powerful modality for imaging and material characterization. Another advantage of THz is this spectrum provides unique spectroscopic information and high resolution.These unique features lead us to use this frequency for medical purposes. As low power sources are used in this frequency regime the sample holder which are used to hold materials such as powdered samples, biological tissues and liquid samples, need to be designed carefully to suppress the inevitable reflections at the interface between the air and sample holder leading to minimum power loss. One way is to make use of transparent THz metamaterial to minimize the losses. In this section multiple layer based bandpass filters with wide band characteristics are presented in THz regime.

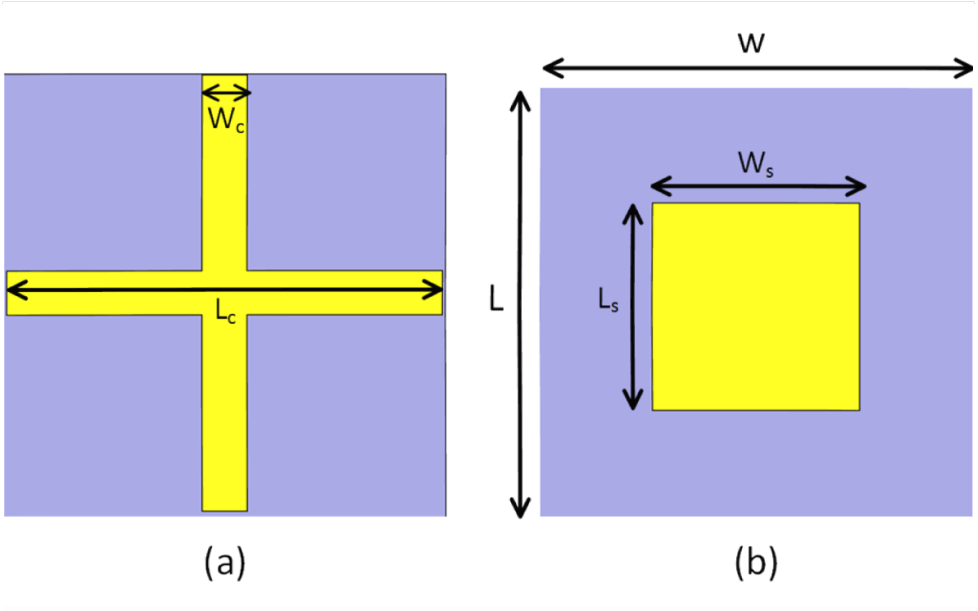

Figure 3.11: FSS bandpass filter consisting of (a) cross structure sandwiched between two (b) square layers.

The main idea in designing FSS with bandpass characteristics is to suppress the reflections by perfect impedance matching of the structure air interface with the of air impedance. Furthermore, in order to have broadband characteristics multiple layer are used for this purpose. First, a multi-layer of printed square and cross structures is discussed, the structures are shown in Figure 3.11 [29]. The side view of structure is shown in Figure 3.12 which consist of a cross being sandwich between two squares. The substrates and superstrates used in for this structure are polyethylene, which has a permittivity of $\epsilon_r = 2.25$ and $\tan\delta = 0.001$, respectively. Table 3.5 shows the physical parameters of unit cell of the design. The transmission and reflection coefficient of this structure at different angle of incidence are shown in Figure 3.13 and Figure 3.14, respectively. At normal incidence the 95% transmission is from 0.62 THz to 0.87 THz (0.25 THz), whereas at off normal incidence (5^o to 15^o) the 95% bandwidth is from 0.64 THz to 0.88 THz (0.24 THz).

A broader transmission bandwidth is achieved when the structures are replaced by a fan type pattern shown in Figure 3.15 [29] [30]. The 3D view and side view of bandpass filter are shown in Figure 3.16 and Figure 3.17, respectively. It also

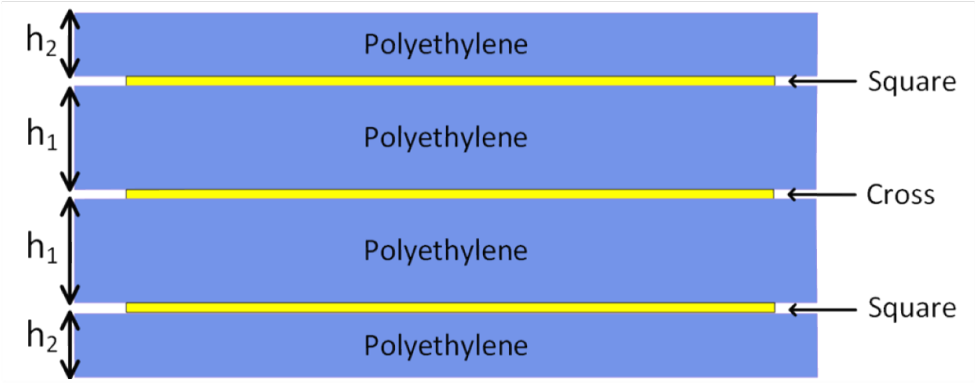

Figure 3.12: Sideview of the multilayer FSS bandpass filter consisting of cross structure being sandwiched between square structures.

Table 3.5: Physical parameters of the multilayer FSS bandpass filter consisting of cross structure being sandwiched between square structures.

Parameters	Values (μm)
L	174
W	174
L_s	81.2
W_s	81.2
L_c	171.1
W_c	17.4
h_1	20
h_2	10

consists of three layers in which the slot metallic layer is sandwiched between printed layers of fan structure. The substrates and superstrates material are same as used for the previous structure. Table 3.6 shows all the parameters of the structure unit cell. The transmission coefficient result at normal incidence is shown in Figure 3.18. The 95% transmission of this design is from 0.74 THz to 1.04 THz (0.3 THz). Figure 3.19 shows transmission at different angle of incidence (0^o to 40^o) and it observable that as the angle of incidence is increasing the 95% transmission bandwidth starts to decrease.

The above two multi layer structures have very good results and are very wide band, however the practical realization and arranging the structures on top of each other is very difficult. First of all, the thickness of substrates vary in the

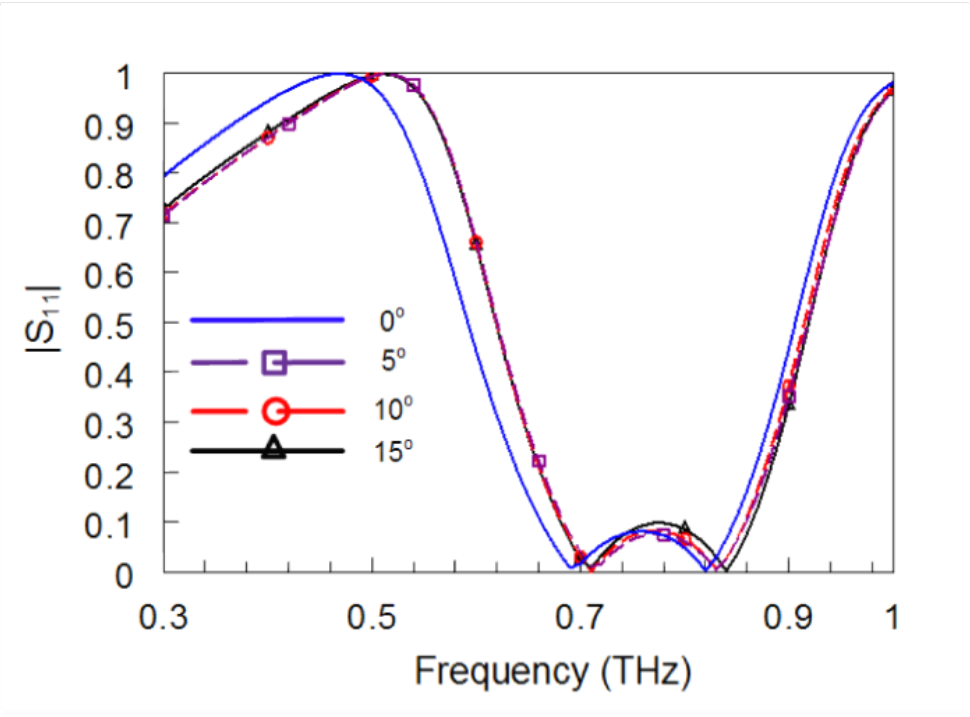

Figure 3.13: FSS simulation results of the reflection coefficient of the multilayer bandpass FSS filter consisting of cross structure, sandwiched between two square layers at different angles of incidence.

range of 3 μm to 20 μm which are very thin substrates. If we fabricate a single thin layer with array of cells on top it, while moving it through different process flow it will have high probability to break. The second issue is the arrangement of the layers on top of each other for that we need high precision of about 1 μm or even less. Even a small error in the arrangement will affect the results tremendously. The third issue is, the air can trap easily in between the multi layers during the fabrication process. The trapped air can change the results significantly, it can shift the desired frequency and it may change the transmission or reflection coefficient since the impedance of unit cell, which is required to be matched to air, will also change with the air gap.

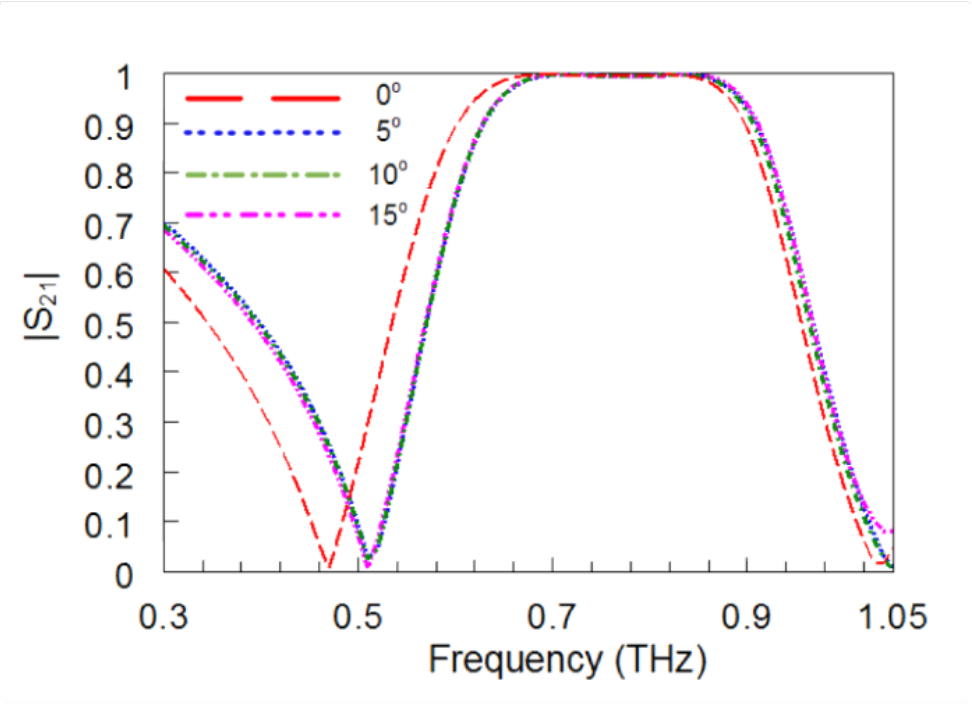

Figure 3.14: HFSS simulation results of the transmission coefficient of multilayer FSS bandpass filter consisting of cross structure, sandwiched between two square layers at different angles of incidence.

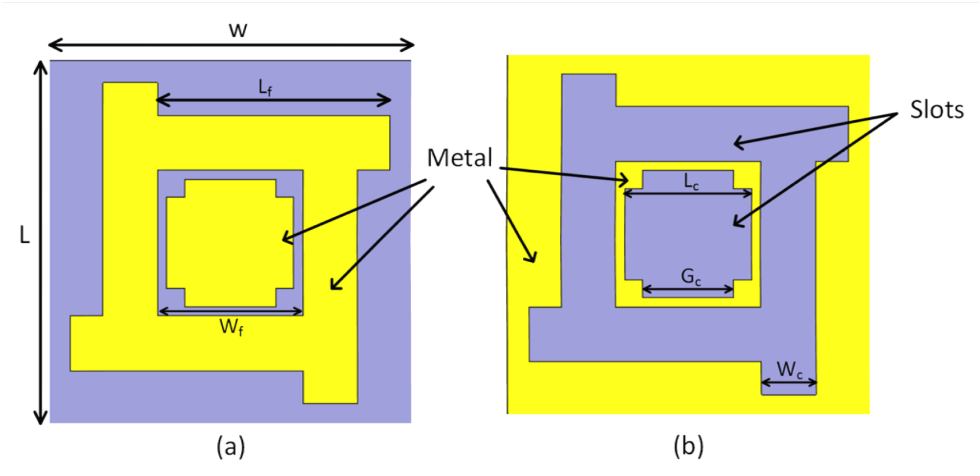

Figure 3.15: Multilayer FSS bandpass filter consisting of (a) Fan printed and (b) Fan Slot patterns.

Table 3.6: Physical geometry parameters of the multilayer FSS bandpass filter consisting of the slot Fan (Figure 3.15(b)) being sandwiched between the printed Fan (Figure 3.15(a)) patterns.

Parameters	Values (μm)
L	70
W	70
L_f	44.8
W_f	28
L_c	24.5
W_c	10.5
G_c	17.5
h_1	15
h_2	3

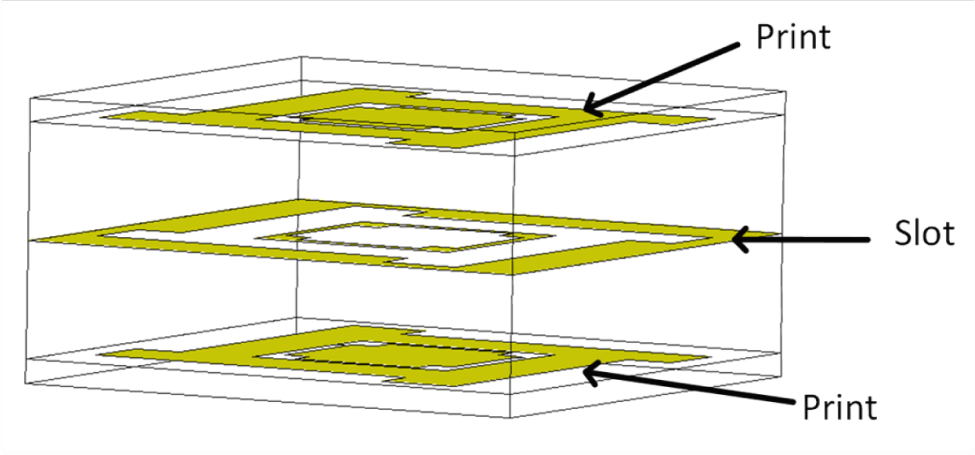

Figure 3.16: 3D view of the multilayer FSS bandpass filter consisting of the slot Fan (Figure 3.15(b)) being sandwiched between the printed Fan (Figure 3.15(a)) patterns.

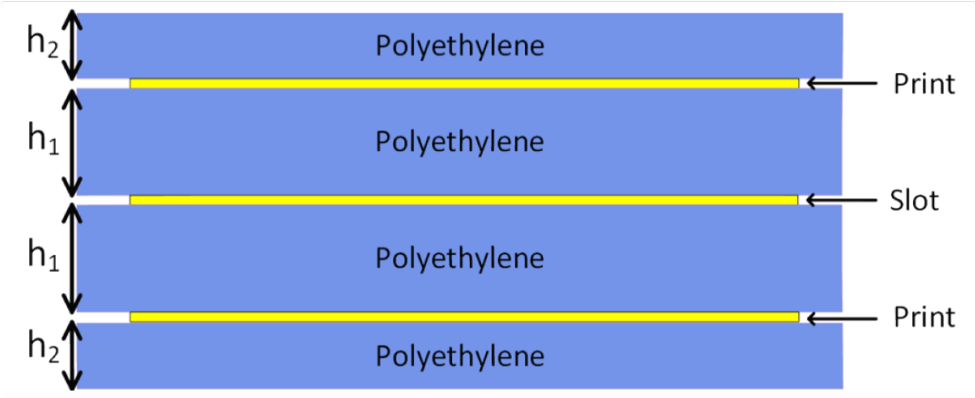

Figure 3.17: Side view of the multilayer FSS bandpass filter consisting of the slot Fan (Figure 3.15(b)) being sandwiched between the printed Fan (Figure 3.15(a)) patterns.

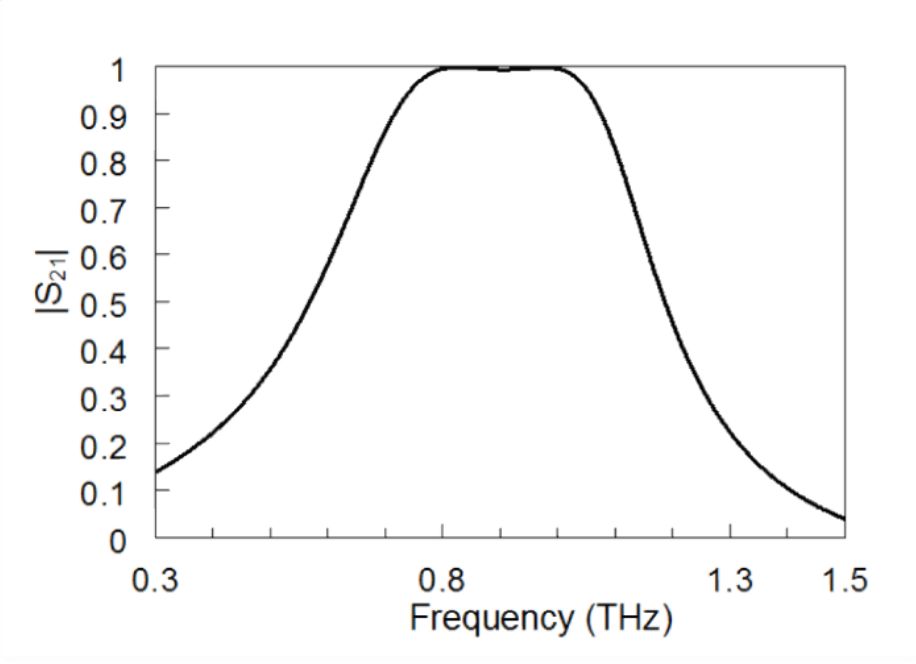

Figure 3.18: HFSS simulation results of the transmission coefficient of the multilayer FSS bandpass filter consisting of the slot Fan (Figure 3.15(b)) being sandwiched between the printed Fan (Figure 3.15(a)) patterns for normal incidence.

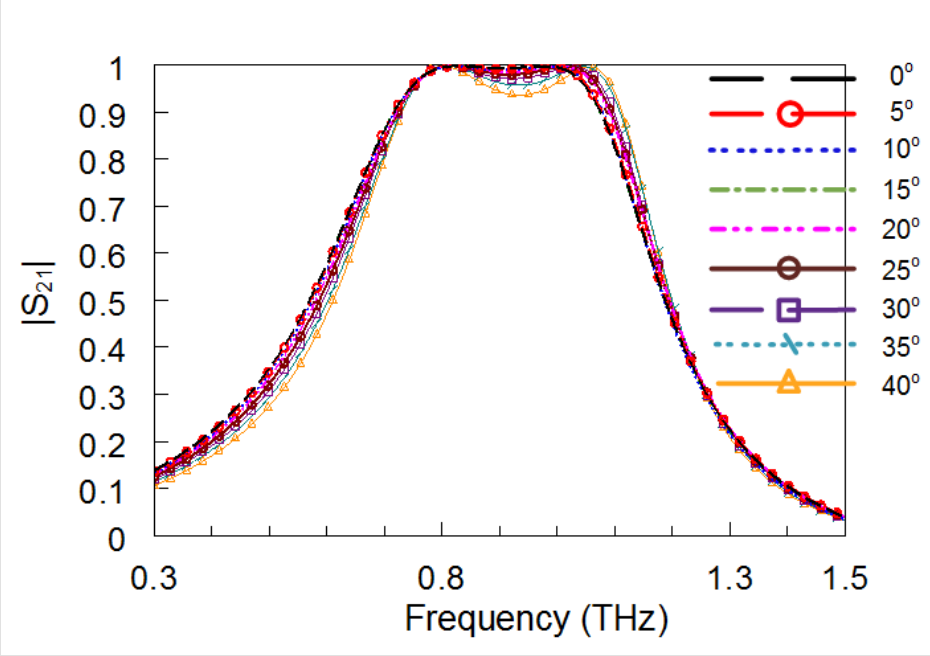

Figure 3.19: HFSS simulation results of transmission coefficient of the multilayer FSS bandpass filter consisting of the slot Fan (Figure 3.15(b)) being sandwiched between the printed Fan (Figure 3.15(a)) patterns for different angles of incidence.

Chapter 4

Single layer bandpass filters

In the previous Chapter, multilayer FSS patterns with broadband characteristics were discussed. Those designs had some sensitive issues such as thin layer of substrates, danger of trapping air gap between the layers and micro alignment of inter layer unit cells. The practical design implementation of these complex structures is very difficult with the available fabrication facilities. The remedy to above constrained is to provide possible and much simpler designs, having bandpass characteristics. The goal of this chapter is to propose single layer FSS bandpass filters whose fabrication process is possible.

Figure 4.1 shows periodic square apertures. If a wave with vertical polarization is incident upon this surface then it can be envisioned as infinitely long rods that can be modeled as inductors across a equivalent transmission line. The horizontal bars will act as capacitors in parallel with the inductor. However, the separation between the horizontal bar is too large due which the equivalent capacitance value is very small to produce any resonance [5].There are numerous ways to increase the capacitance to have bandpass characteristics. The simplest way is to place a solid metallic plate inside each aperture to decrease the distance between the horizontal bars in order to increase the capacitance. This will produce a more strong resonance at a lower frequency. Using this approach, number of single layer bandpass structures are presented whose fabrication is much simple and

more realizable in practical life.

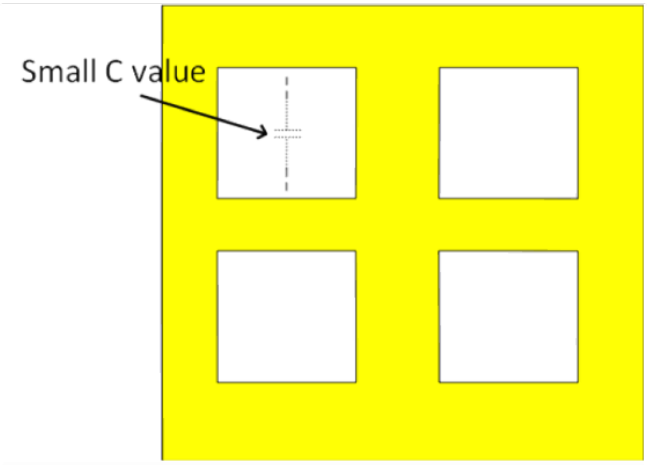

Figure 4.1: Metallic sheet with square apertures .

For all of the proposed single layer bandpass FSS patterns, pyrex glass is used as the substrate with the permittivity of ϵ_r=4.6. It is available with a standard thickness of approximately 500 μm. In HFSS simulations, 100 μm thick Pyrex glass membranes are used for different structures. Finally, the fabrication process is explained in which it will be elaborated more on how to realize the fabrication of these structures on such a thin film substrate of Pyrex glass.

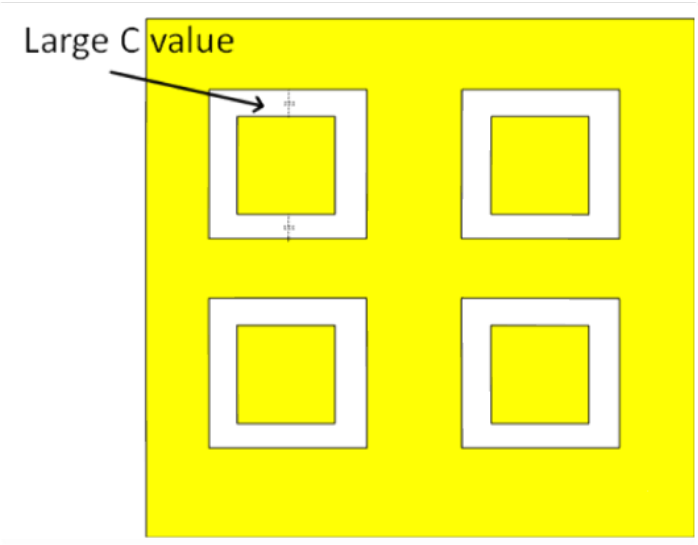

Figure 4.2: Metallic sheet with square apertures loaded with square metals .

4.1 Circular aperture loaded with metallic circular disc bandpass FSS

This structure consist of circular aperture loaded with metallic circular disk to achieve bandpass characteristics. Figure 4.3 shows the top and side view of unit cell of the structure. The unit cell is developed on 100 μm pyrex glass substrate. The unit cell structure parameters are given in Table 4.1.

Table 4.1: Physical geometry parameters of the circular ring slot as a bandpass filter.

Parameters	Values (μm)
R_{in}	43
R_{out}	45
D_x	100
D_y	100
h	100

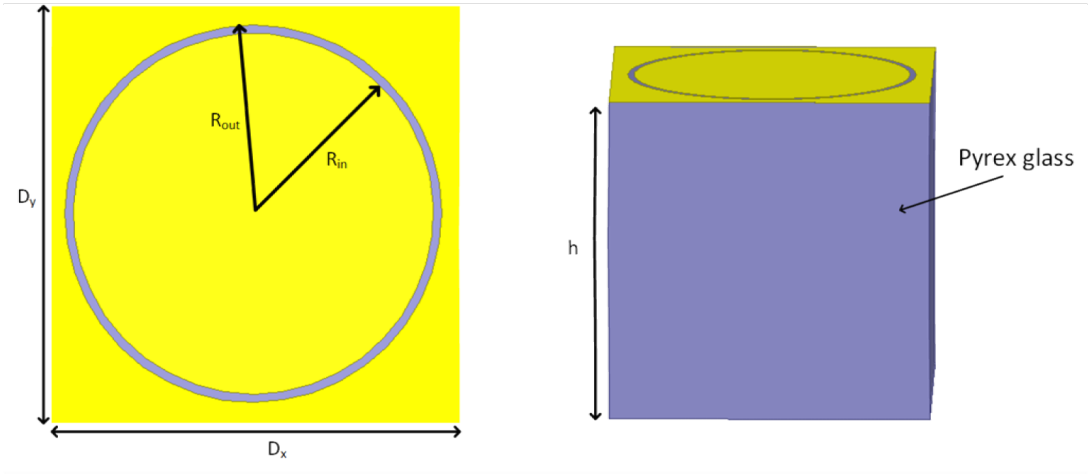

Figure 4.3: Single layer bandpass FSS filter consisting of a circular ring slot inside a square metal.

The transmission coefficient results at normal incidence are given in Figure 4.4. The transmission center frequency is around 0.68 THz with 95% transmission bandwidth from 0.658 THz to 0.7 THz (0.042 THz). Figure 4.5 shows simulation results of transmission coefficient at different angles incidence, the structure 95%

bandwidth remain almost same till 40^o after that it starts to decrease. However, the maximum transmission remain close to unity at all angle of incidence.

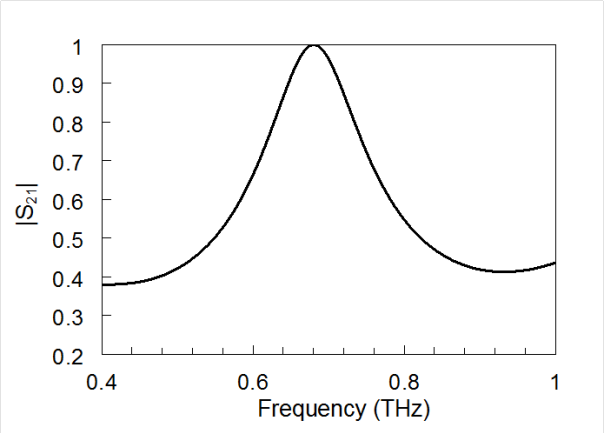

Figure 4.4: HFSS simulation results of the transmission coefficient of the single layer bandpass FSS filter consisting of a circular ring slot inside a square metal at normal incidence.

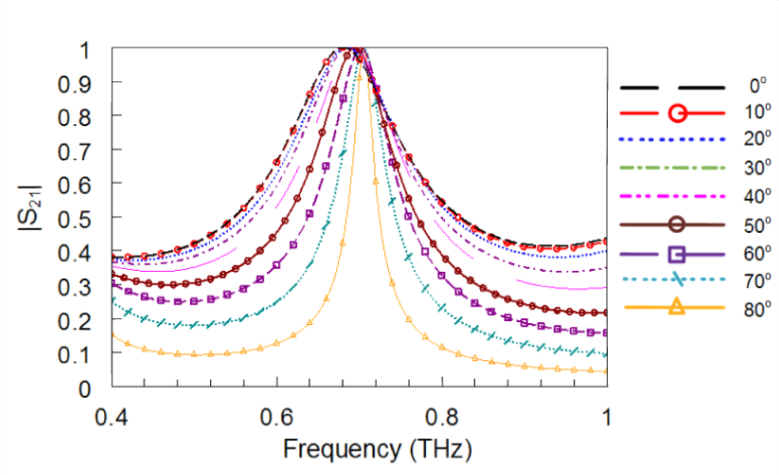

Figure 4.5: HFSS simulation results of the transmission coefficient of the single layer bandpass FSS filter consisting of a circular ring slot inside a square metal at different angles of incidence.

4.2 Tripole FSS structure

Figure 4.6 shows the unit cell structure and side view of tripole structure. The triple is designed and optimized for 0.8 THz frequency. The length and width of tripole and each unit cell length and width parameters in μm scale are given in Table 4.2. The tripole is designed on same pyrex glass with thikcness of 100 μm.

Table 4.2: Physical geometry parameters of the single layer tripole bandpass FSS filter.

Parameters	Values (μm)
W_1	3
W_2	8
L	40
D_x	100
D_y	100
h	100

The transmission coefficient results at normal incidence are given in Figure 4.10. The 95% bandwidth is from 0.794 THz to 0.809 THz (0.015 THz). The structure response at different angle of incidence is also observed. Figure 4.8 shows the transmission coefficient results at different angles from 0^o to 80^o. The 95% transmission bandwidth remains approximately the same till 30^o angle of incidence of the wave. As the angle of incident wave is increased beyond that the transmission coefficient bandwidth becomes narrower and narrower, however the maximum amplitude does not go below 97%.

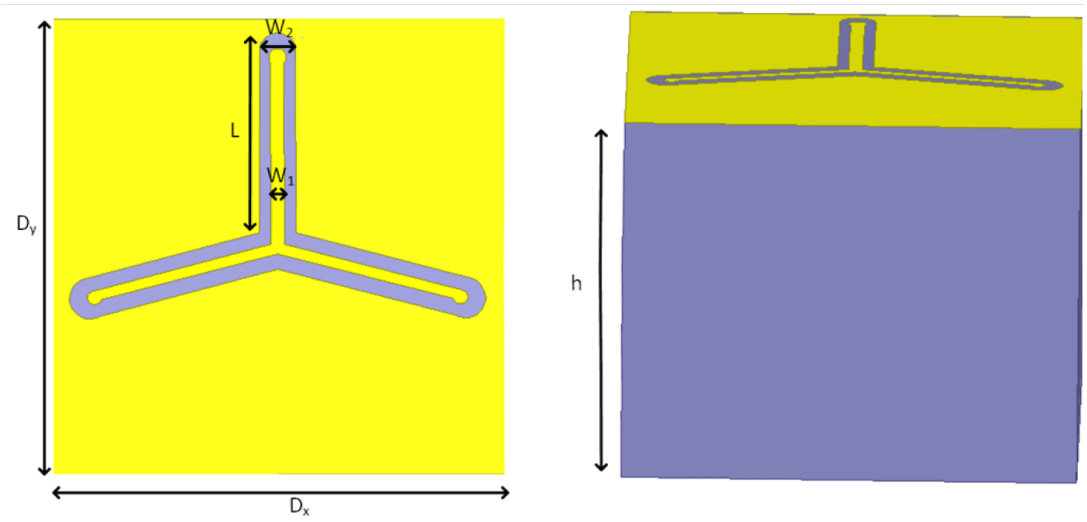

Figure 4.6: The unit cell of the single layer tripole bandpass FSS structure.

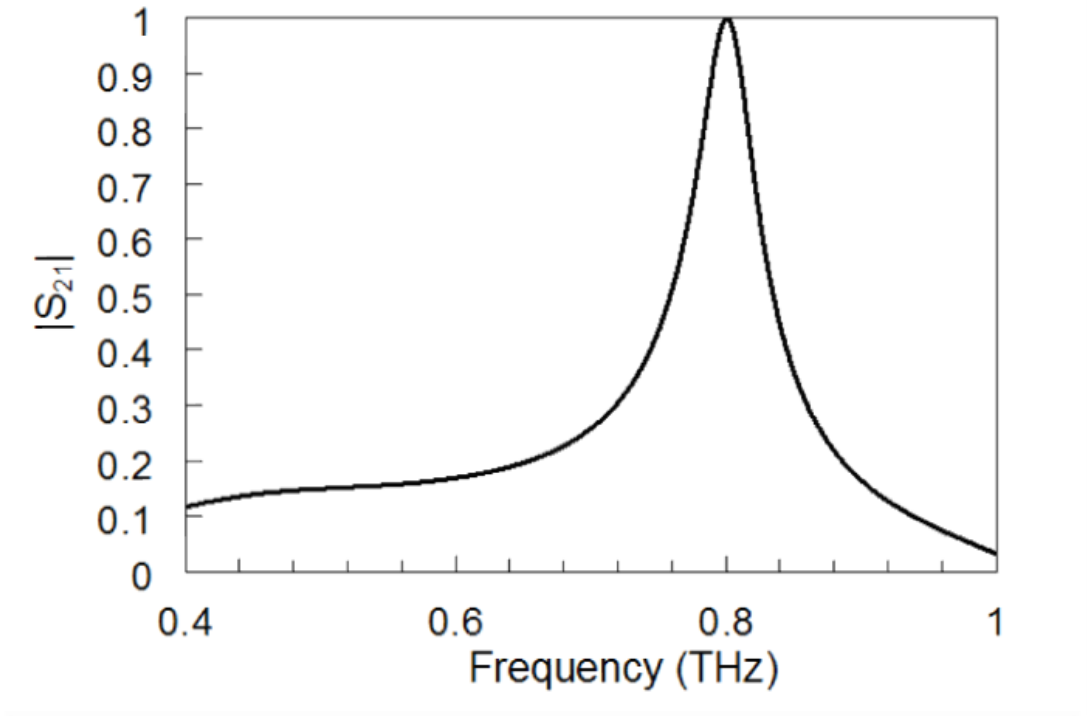

Figure 4.7: HHFSS simulation results of the transmission coefficient of single layer tripole bandpass FSS filter at normal incidence.

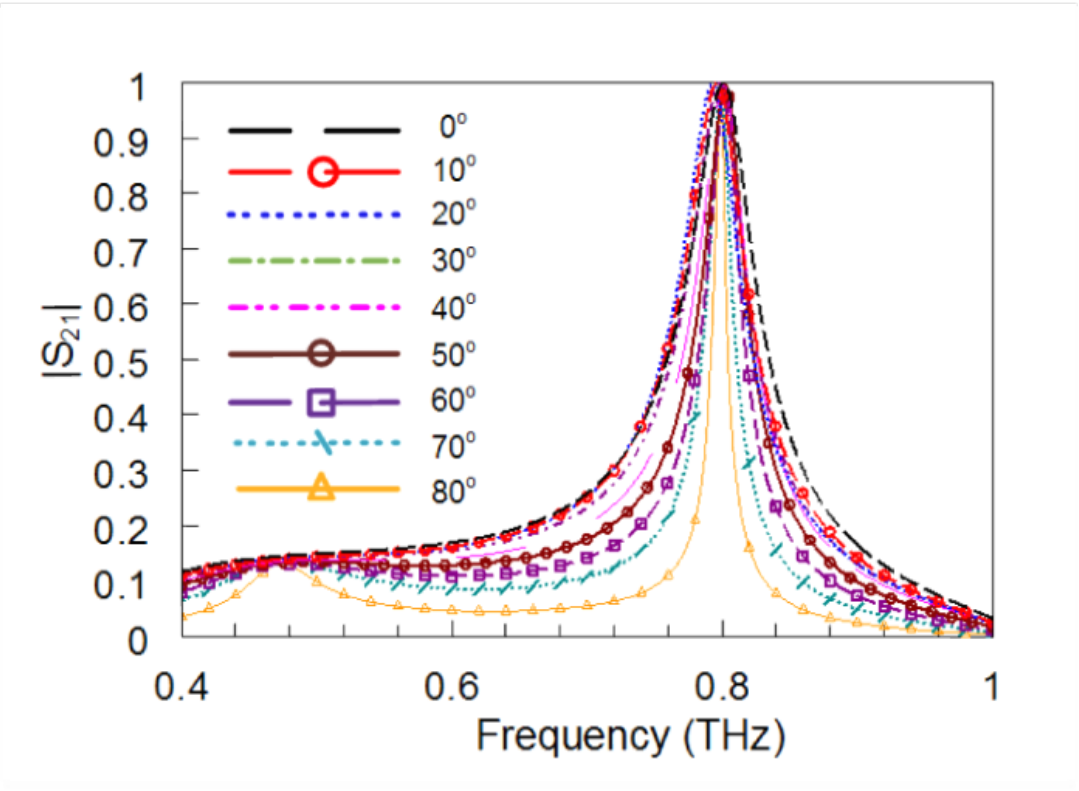

Figure 4.8: HFSS simulation results of the transmission coefficient of the single layer tripole bandpass FSS structure at different angles of incidence.

4.3 Triangular FSS structure

Figure 4.9 shows the unit cell structure and side view of triangular slot structure. The triangle is designed and optimized for 0.8 THz frequency. The side lengths and both widths of tripole and each unit cell length and width parameters in μm scale are given in Table 4.3. The triangular slot structure is designed on same pyrex glass with thickness of 100 μm.

The transmission coefficient results at normal incidence are given in Figure 4.10. The 95% bandwidth is from 0.791 THz to 0.806 THz (0.015 THz). The structure response at different angle of incidence is also observed. Figure 4.11 shows the transmission coefficient results at different angles from 0^o to 80^o. The 95% transmission bandwidth remains approximately the same till 20^o angle of incidence of the wave. As the angle of incident wave is increased beyond that the

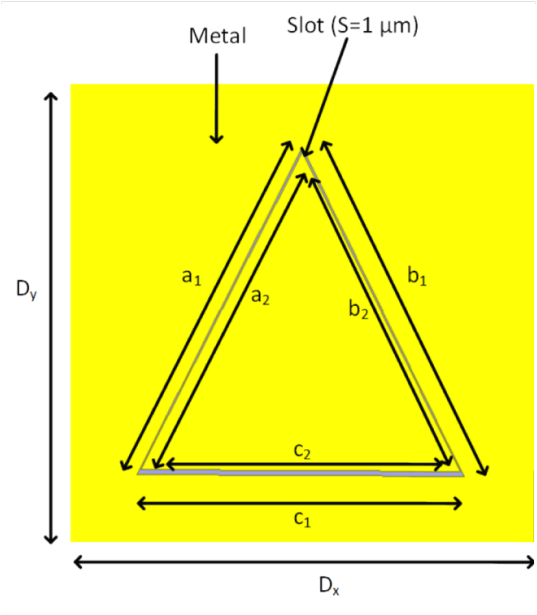

Figure 4.9: The unit cell of single layer bandpass FSS filter consists of a triangular slot inside a square metal.

transmission coefficient bandwidth becomes narrower and narrower and in this case the maximum amplitude also starts to decreasing.

Table 4.3: Physical parameters of the single layer bandpass FSS filter consists of a triangular slot inside a square metal.

Parameters	Values (μm)
a_1	78.3
a_2	76.02
b_1	76.02
b_2	76.02
c_1	70
c_2	68
D_x	100
D_y	100
h	100

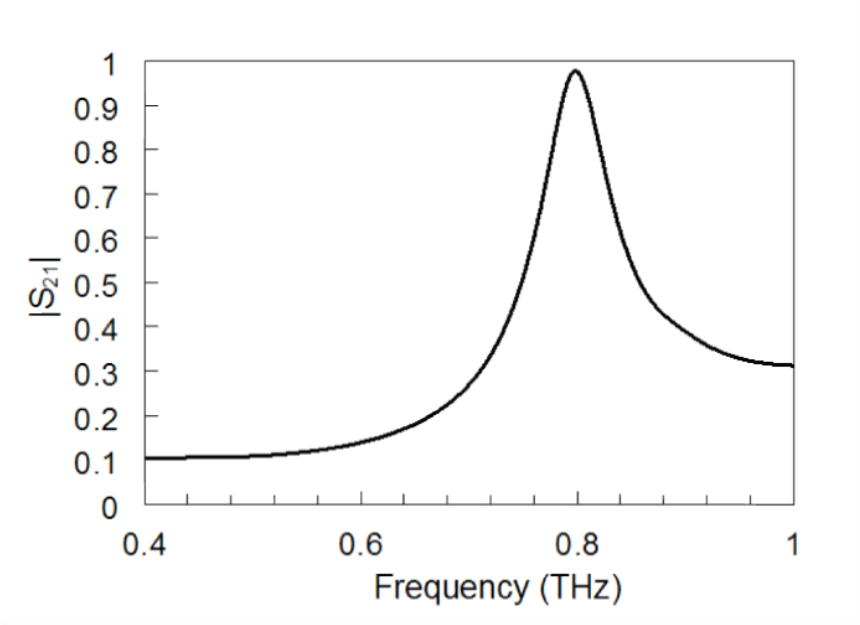

Figure 4.10: HFSS simulation results of the transmission coefficient of the single layer bandpass FSS filter consisting of a triangular slot inside a square metal at normal angle of incidence.

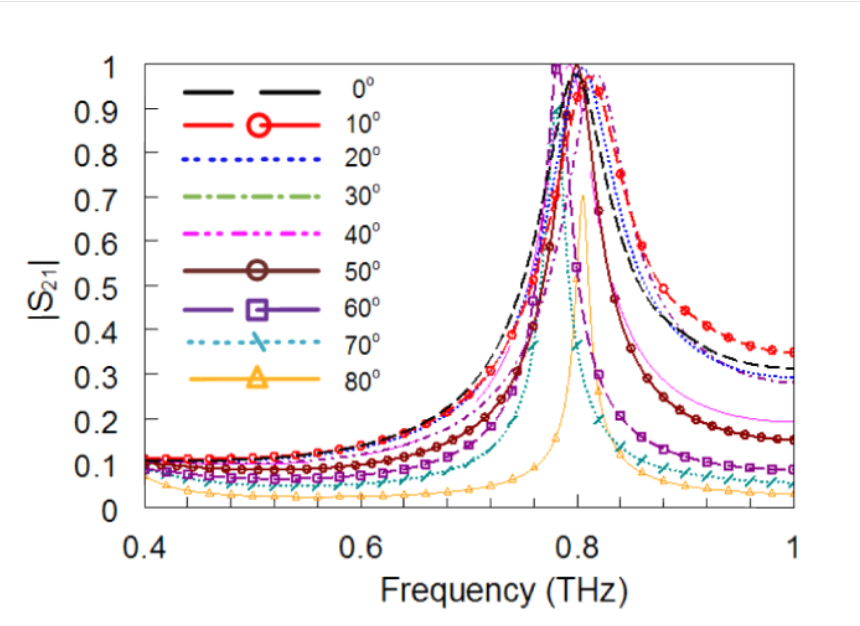

Figure 4.11: HFSS simulation results of the transmission coefficient of the single layer bandpass FSS filter consisting of a triangular slot inside a square metal at different angles of incidence.

4.4 Fabrication process flow using microfabrication techniques

Many industries such as solar panel, optoelectronics, flat screen display and microsystem/MEMS make use microfabrication techniques to design their devices. In the plane the typical dimensions are around 1 μm. Vertical dimensions range from atomic-layer thickness (0.1 nm) to hundreds of micrometres but thicknesses from 10 nm to 1 μm are typical [31]. In this chapter, the fabrication flow of the structure is discussed by using pyrex glass as the substrate for the design. The fabrication consists of a number of steps of lithography, deposition and etching.

4.4.1 Etching

The process pattern transfer consist of two steps lithographic resist patterning and the subsequent etching of the underlying material [31]. Based on the profile, etching is divided into categories as isotropic and anisotropic etching. In isotropic etching case, it etches equally in all directions so it has more curve profile and is not directional. Anisotropic etching is directional so its profile somewhat vertical. In this thesis, wet etching is used which has profile similar to isotropic etching.

4.4.2 Liftoff process

Liftoff process is used to remove unwanted deposited metal to have the desired patterns on the top of the substrate. In this process, initially photo resist is coated and patterned accordingly. After that the metal is deposited, the deposited metal at the top of photo resist is removed with the help of a developer such as acetone as results at last we are only left with desired metallic patterns.

4.5 Fabrication process of FSS

For the design project, a Pyrex glass is used as the substrate which is commercially available with a thickness of about 500 μm. However, using 500 μm thickness of substrate affect the results. For this reason, substrate is etched from beneath to the required design thickness of 100 μm. In order to provide mechanical support membrane, the periphery of FSS is kept at 100 μm thickness. To realize the designs, a fabrication process flow is defined as given below.

Initially we have 500 μm-thick Pyrex glass (Figure 4.12(a)), the patterns are generated in the area in between the supporting anchor points of the membrane so that the maximum transmission coefficient results are not affected too much. For pattern generation, photoresist is coated on top of the substrate (Figure 4.12(b)). Since we want to use liftoff process for pattern generation, the photoresist is exposed to UV light with the mask aligner and left in developer to make empty spaces for pattern generation (Figure 4.12(c)). After the lithography process, the Cr/Au is deposited on top of the substrate using thermal evaporation and it occupies the empty spaces (Figure 4.12(d)). In order to remove the unwanted metal on top of photoresist, the sample is kept in a developer such as acetone which removes all the unwanted metal. At last we will be left with the patterns of the unit cells (Figure 4.12(e)).

After pattern generation, we need to decrease the thickness of the glass to 100 μm using wet etching with an etchant such as HF. Since HF is very active against photoresist it cannot be used as a protection layer during the glass etching. For Pyrex glass etching Cr/Au/Cr/Au is used for protecting the anchors from etching. In etching process of Pyrex glass, patterns are defined with the photoresist using double sided alignment process (Figure 4.13(f)). After that using mask aligner and developing methods, photoresist is removed from the regions to be protected in glass etching. (Figure 4.13(g)). Cr/Au/Cr/Au is deposited (Figure 4.13(h)). The sample is kept in acetone for removing unwanted metal deposited on the top of photoresist (Figure 4.13(i)). After the liftoff process, only the glass anchor region to be protected are covered with Cr/Au/Cr/Au. The backside of the

sample is protected from etching using a wafer holder. As HF-dip is a wet etching process, the etching profile will be isotropic. Depending on the total time of the glass etching in HF, we will be left with 100 μm thick membrane below the unit cells (Figure 4.13(j)). Finally, Cr/Au/Cr/Cr is removed using Cr/Au etchants and we will be left with the four 500 μm-thick anchor points at the edges of the substrates which will give mechanical support to the end product and make the design more robust (Figure 4.13(k)).

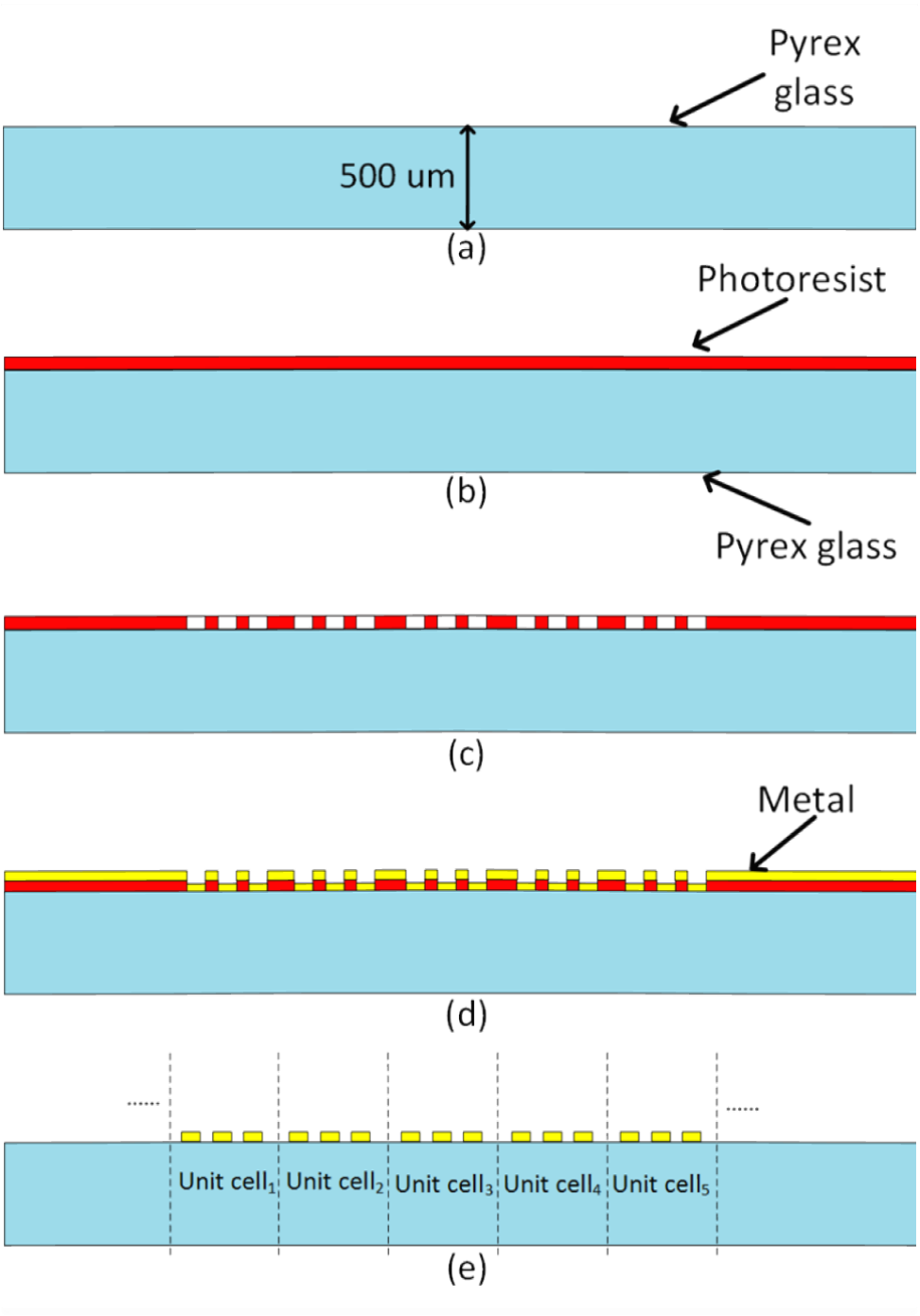

Figure 4.12: Fabrication process flow, (a) A Pyrex glass substrate with 500 μm thickness, (b) Spin coating of photoresist, (c) Patterning the photoresist for liftoff process, (d) Deposition of the metal, and (e) After liftoff only unit cell patterns are left.

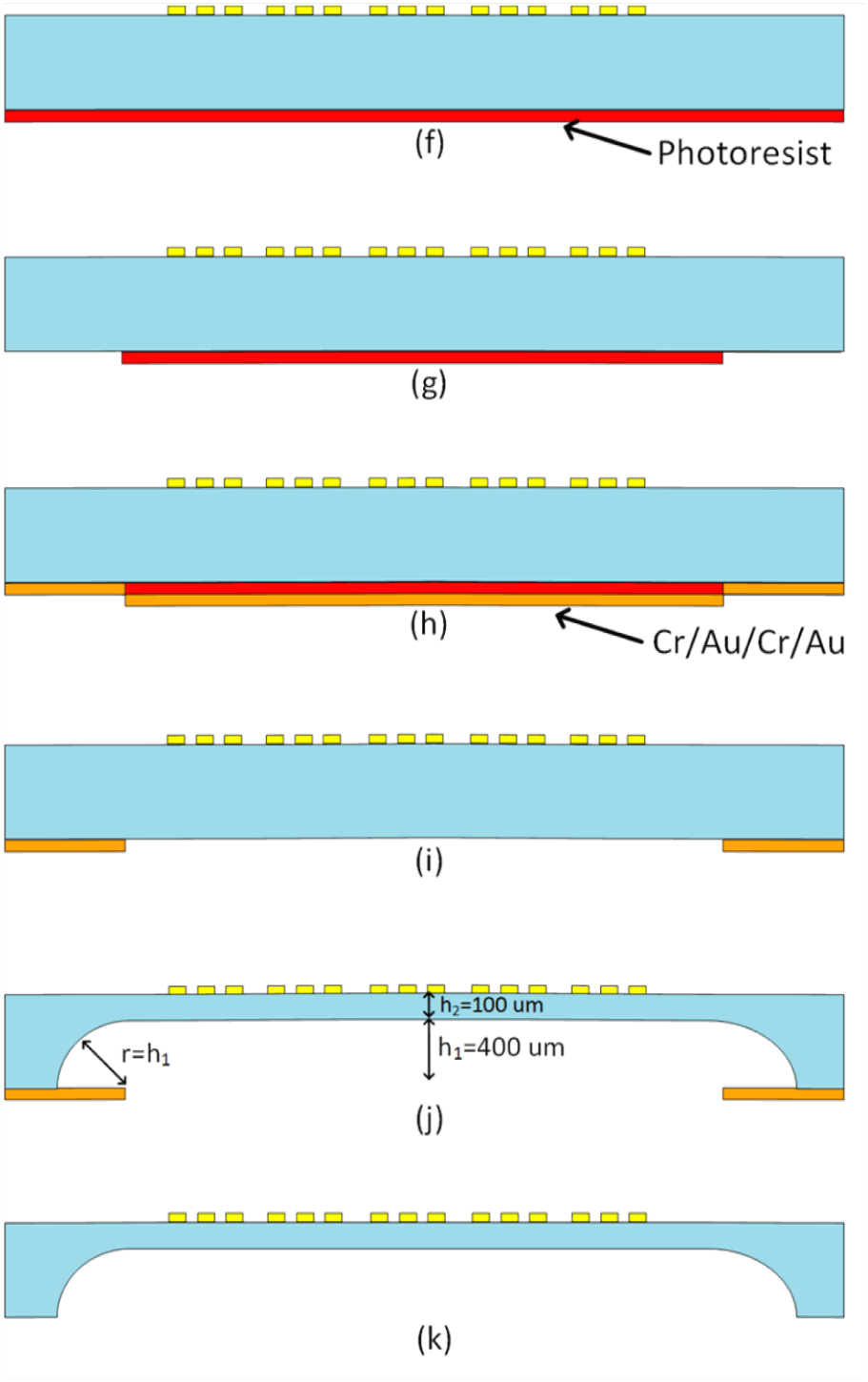

Figure 4.13: Fabrication process flow (etching of pyrex glass) (f) Spin coating of the photoresist, (g)Patterning the photoresist for the liftoff process, (h)Deposition of Cr/Au/Cr/Au (i)Liftoff process using acetone (j)Wet etching of the lower side of Pyrex glass using HF while the other side is protected with a wafer holder, and (k)100 μm thick Pyrex glass membrane with patterns.

Chapter 5

Conclusion

In conclusion, three single layer bandpass filters are proposed with performances of more than 95% max transmission coefficient and their results are also independent of angle of incidence to certain ranges of degrees. Single layer bandpass frequency selective surfaces are preferred over multilayer, which suffer from thin layer of substrates, micro alignment of unit cells and trapped air gap between the layers in THz spectrum. Although the bandwidth of a single layer FSS is less than that of a multilayer FSS, robustness and practical implementation of single layer surpasses the multilayer. A simple and acceptable fabrication process flow is proposed for single thin layer FSS and these fabrication steps are compatible with the facilities available at UNAM.

As a future work, the practical implementation of these single layer structure will be accomplished and furthermore they will be measured soon with the currently developing measurement setup at UNAM. Furthermore, more research can be conducted on how to increase the bandwidth of the FSS whose fabrication process should be realizable with the available equipment. Apart from that, a detail research can be conducted on better fabrication process flows for multilayer structures which provide robustness to each layer of structure with best alignment of unit cells and minimum air gap between the layers.

The current fabrication technique can be used for the designing of multilayers. However, the four corner anchor points inevitably introduce 400 μm of air gap between the layers which shift the frequency and introduce ripples in the results. In future, the thickness of anchor points can be reduced, which will allow use to reduce the air and may be it can lead us to matching of the structure over a wide band using multilayer configuration. The shape of the structure and inter-element spacing play important role in deciding the bandwidth and making the array independent of angle of incidence to wide range. Special research can be done on compact and tightly packed elements yielding much better performances.

Bibliography

[1] S. Fernandez, "Frequency selective surfaces for terahertz applications," November 2012. [Online]. Available: https://www.era.lib.ed.ac.uk/handle/1842/7648.

[2] R. Ulrich, "Far-infrared properties fo metallic mesh and its complementary structure," *Infrared Phys.*, no. 7, pp. 37 – 55, 1967.

[3] S. W. Lee, G. Zarrillo, and C. L. Law, "Simple formulas for transmission through periodic metal grids or plates," *IEEE Transactions on Antennas and Propagation*, pp. 904 – 909, 1982.

[4] T. Wu, *Frequency selective surface and grid array.* John Wiley & Sons, 1995.

[5] B. A. Munk, *Frequency selective surfaces theory and design.* John Wiley & Sons, 2000.

[6] P. H. Siegel, "Terahertz technology," *IEEE transactions on microwave theory and techniques*, vol. 50, no. 3, pp. 910 – 928, 2002.

[7] Y. Sun, M. Y. Sy, Y.-X. J. Wang, A. T. Ahuja, and Y.-T. Zhang, "A promising diagnostic method: Terahertz pulsed imaging and spectroscopy," *World Journal of W J R Radiology*, pp. 55– 65, 2011.

[8] M. C. Kemp, P. F. Taday, B. E. Cole, J. A. Cluff, A. J. Fitzgerald, and W. R. Tribe, "Security applications of terahertz technology," *Proc. of SPIE*, vol. 50, no. 3, pp. 44 – 52, 2008.

[9] A. Redo-Sanchez and X.-C. Zhang, "Terahertz science and technology trends," *IEEE journal of selected topics in quantum electronics*, vol. 14, no. 2, pp. 260 – 269, March 2008.

[10] C. Corsi and F. Sizov, *THz and Security Applications: Detectors, Sources and Associated Electronics*. Springer, 2014.

[11] P. H. Siegel, "Terahertz technology in biology and medicine," *IEEE Transactions on Microwave Theory And Techniques*, vol. 52, no. 10, pp. 2438–2447, 2011.

[12] V. Sanphuang, W. G. Yeo, J. L. Volakis, and N. K. Nahar, "Thz transparent metamaterials for enhanced spectroscopic and imaging measurements," *IEEE Transactions on Terahertz Science And Technology*, vol. 5, pp. 117–122, January 2015.

[13] S. Vegesna, Y. Zhu, A. Bernussi, and M. Saed, "Terahertz two-layer frequency selective surfaces with improved transmission characteristics," *IEEE Transactions On Terahertz Science And Technology*, vol. 2, pp. 441 – 448, July 2012.

[14] F. Bayatpur and K. Sarabandi, "Single-layer high-order miniaturized-element frequency-selective surfaces," *IEEE Transactions On Microwave Theory And Techniques*, vol. 56, pp. 774 – 781, July 2012.

[15] S. Mahashabde, A. Sobolev, A. Bengtsson, D. Andren, M. A. Tarasov, M. Salatino, P. de Bernardis, S. Masi, and L. S. Kuzmin, "A frequency selective surface based focal plane receiver for the olimpo balloon-borne telescope," *IEEE Transactions On Terahertz Science And Technology*, vol. 5, pp. 145 – 152, January 2015.

[16] J. P. Creen and D. Veron, "Theory of the transmission of metal strip gratings on a dielectric substrate application to submillimeter laser coupling," *International Journal of Infrared and Millimeter Waves*, vol. 7, pp. 117– 122, January 1986.

[17] L. B. Whitbourn and R. C. Compton, "Equivalent circuit formulas for metal grid reflectors at a dielectric boundary," *Applied Optics*, vol. 24, pp. 217 – 220, January 1985.

[18] B. Hooberman, "Everything you ever wanted to know about frequency-selective surface filters but were afraid to ask," May 2005. [Online]. Available: http://cosmology.phys.columbia.edu/groupweb/aboutus/memos/hooberman filtersmemo.pdf.

[19] R. C. Compton, L. B. Whitbourn, and R. C. McPhedran, "Near millimeter wave bandpass filters," *Applied Optics*, vol. 23, pp. 3236 – 3242, September 1984.

[20] J. Lesurf, *Millimetre-wave Optics, Devices & Systems*. IOP Publishing Ltd, 1990.

[21] S. T. Shanahan and N. R. Heckenberg, "Transmission line model of substrate effects on capacitive mesh couplers," *Applied Optics*, vol. 20, pp. 4019 – 4023, December 1981.

[22] T. Timusk and P. L. Richards, "Near millimeter wave bandpass filters," *Applied Optics*, vol. 20, pp. 1356 – 1359, April 1981.

[23] H. Tao, C. M. Bingham, A. C. Strikwerda, D. Pilon, D. Shrekenhamer, N. I. Landy, K. Fan, X. Zhang, W. J. Padilla, and R. D. Averitt, "Highly flexible wide angle of incidence terahertz metamaterial absorber: Design, fabrication, and characterization," *Phys. Rev. B*, vol. 78, no. 18, pp. 241103–1 – 241103–4, December 2008.

[24] J. B. Pendry, "Negative refraction makes a perfect lens," *Phys Review Letters*, vol. 5, no. 18, pp. 3966 – 3969, October 2000.

[25] D. Schurig, J. J. Mock, B. J. Justice, S. A. Cummer, J. B. Pendry, A. F. Starr, and D. R. Smith, "Metamaterials electromagnetic cloak at microwave frequencies," *Science*, vol. 314, pp. 977 – 980, November 2006.

[26] J. L. Volakis, G. Mumcu, K. Sertel, C. C. Chen, M. L. B. Kramer, D. Psychoudakis, and G. Kiziltas, "Antenna miniaturization using magnetic-photonic and degenerate band-edge crystals," *IEEE Antennas Propag Mag*, vol. 48, no. 5, pp. 12 – 28, October 2006.

[27] C. M. Soukoulis and M. Wegener, "Past achievements and future challenges in the development of three-dimensional photonic metamaterials," *Nature Photonics*, vol. 5, pp. 523 – 530, July 2011.

[28] W.-G. Yeo, N. K. Nahar, and K. Sertel, "Far-ir multiband dual polarization perfect absorber for wide incident angles," *Microwave and Optical Technology Letters*, vol. 55, no. 3, pp. 632 – 636, March 2013.

[29] W.-G. Yeo, V. Sanphuang, N. K. Nahar, and J. L. Volakis, "Thz periodic surfaces to enhance spectroscopic measurements," *IEEE International Conference on Electromagnetics in Advanced Applications*, pp. 924 – 925, 2012.

[30] M. C. Kemp, P. F. Taday, B. E. Cole, J. A. Cluff, A. J. Fitzgerald, and W. R. Tribe, "Broadband thz filters for thz sensing devices," *IEEE National Aerospace and Electronics Conference*, pp. 38 – 39, 2012.

[31] S. Franssila, *Introduction to Micro fabrication*. John Wiley & Sons, 2004.